Available online at www.sciencedirect.com
ScienceDirect
Journal of Computational Physics 224 (2007) 785–823
JOURNAL OF COMPUTATIONAL PHYSICS
www.elsevier.com/locate/jcp

A cell-centered diffusion scheme on two-dimensional unstructured meshes

Jérôme Breil, Pierre-Henri Maire *

UMR CELIA, CEA–CNRS–Université Bordeaux I, 33405 Talence Cedex, France

Received 28 June 2006; received in revised form 10 October 2006; accepted 18 October 2006
Available online 28 November 2006

Abstract

We propose a new cell-centered diffusion scheme on unstructured meshes. The main feature of this scheme lies in the introduction of two normal fluxes and two temperatures on each edge. A local variational formulation written for each corner cell provides the discretization of the normal fluxes. This discretization yields a linear relation between the normal fluxes and the temperatures defined on the two edges impinging on a node. The continuity of the normal fluxes written for each edge around a node leads to a linear system. Its resolution allows to eliminate locally the edge temperatures as function of the mean temperature in each cell. In this way, we obtain a small symmetric positive definite matrix located at each node. Finally, by summing all the nodal contributions one obtains a linear system satisfied by the cell-centered unknowns. This system is characterized by a symmetric positive definite matrix. We show numerical results for various test cases which exhibit the good behavior of this new scheme. It preserves the linear solutions on a triangular mesh. It reduces to a classical five-point scheme on rectangular grids. For non orthogonal quadrangular grids we obtain an accuracy which is almost second order on smooth meshes.

Keywords: Diffusion equations; Cell-centered scheme; Unstructured meshes

1. Introduction

The main goal of this paper is the description and investigation of a new finite volume scheme for solving diffusion equations on two-dimensional unstructured grids. Our scheme is primarily intended for use in applications where occur a strong coupling with a cell-centered hydrodynamic scheme. Therefore, we have developed a robust, cell-centered diffusion scheme, which provides accurate results even on highly distorted grids. Before describing the main features of our new algorithm, let us briefly give an overview of the existing cell-centered diffusion schemes.

It is well known, see [8], that the standard finite volume algorithms, such as the five-point scheme, behave poorly on highly skewed quadrilateral grids. The diffusion front takes on the shape of mesh distortions. This

* Corresponding author.
E-mail address: maire@celia.u-bordeaux1.fr (P.-H. Maire).

0021-9991/$ - see front matter © 2006 Elsevier Inc. All rights reserved.
doi:10.1016/j.jcp.2006.10.025

undesirable behavior is due to the crude finite difference approximation used for discretization of the face fluxes.

Kershaw, in his pioneering work [10] has proposed a nine-point scheme on structured quadrilateral grids, which partially resolves the above mentioned difficulties. His scheme consists of a cell-centered variational method based on a smooth mapping between the logical mesh coordinates and the spatial coordinates. This algorithm reduces to the classical five-point scheme on an orthogonal grid. In addition, it leads to a diffusion matrix, which is symmetric positive definite. Although this method is restricted to structured quadrilateral grids, it has been successfully used in many Lagrangian codes, see [19]. However, the assumption of a smooth mapping used by Kershaw is too restrictive. As it has been shown in [17], a mesh refinement with Kershaw's scheme does not give a convergent solution unless the mesh becomes smooth as it is refined. Moreover, it appears that the normal flux continuity across cell interfaces is not ensured.

These drawbacks have motivated the work of Morel and his co-authors. In [17] they developed a cell-centered diffusion scheme, which treats rigorously material discontinuities and gives a second order accuracy regardless of the smoothness of the mesh. However, this scheme has two disadvantages: there are cell-edge unknowns in addition to the cell-centered unknowns and the diffusion matrix is asymmetric.

A significant improvement was provided by Shashkov and Steinberg. In [25,24] they derived an algorithm using the Support Operators Method (SOM), also named *mimetic finite difference method*. This method, see [23], constructs discrete analogs of the divergence and flux operators that satisfy discrete analogs of important integral identities relating the continuum operators. By this way, the discrete flux operator is the negative adjoint of the discrete divergence in an inner scalar product weighted by the inverse conductivity. This SOM diffusion scheme gives the second order accuracy on both smooth and non smooth meshes either with or without material discontinuities. It has a non local stencil and a dense symmetric positive definite matrix representation for the diffusion operators. The introduction of both cell-centered and face-centered unknowns in [18] leads to a variant of this scheme, which has a local stencil. Many extensions of this algorithm have been recently developed. One can find in [9,12,14] developments that take account non-isotropic materials, polygonal and non-conformal meshes.

In [20], the authors present mimetic preconditioners for mixed discretizations of the diffusion equation. In this paper, SOM is used with two fluxes per edge in order to construct the local flux discretization. Recently, Lipnikov, Shaskov and Yotov developed a local flux mimetic finite difference method in [15], which is very similar to our derivation. They also use two degrees of freedom per edge to approximate the flux. They obtained a symmetric, cell-centered finite difference scheme. Moreover, they demonstrated theoretically the second order convergence for the temperature in the case of simplicial meshes.

In [2,3,1] Aavatsmark and co-authors have proposed an alternative approach named Multi-Point Flux Approximation (MPFA). There, the flux is approximated by a multi-point flux expression based on transmissibility coefficients. These coefficients are computed using continuity of the flux and the temperature across the cell interfaces. This method has only cell-centered unknowns and a local stencil. In [11], Klausen and Russel present the relationships between the Mixed Finite Element Method (MFEM), the Control Volume Mixed Finite Element Method (CVMFEM), the SOM and the MPFA. The latter can be applied in the physical space to quadrilateral and to unstructured grids. For quadrilaterals, which are not parallelograms the MPFA provides a second order scheme [4] but the diffusion matrix is non-symmetric. In [5], the authors develop a MPFA method for quadrilateral grids in the reference space and its relationship to the MFEM. This approach yields a system of equations with a symmetric matrix. It shows a second order convergence on smooth distorted grids. However for rough grids the reference space method suffers the reduction or loss of convergence.

The relation between the finite volume and the MFEM is also studied by Thomas and Trujillo in [27]. These authors use a sub-triangulation, identical to the one used in the present paper. They are also able to eliminate auxiliary unknowns. However, the degrees of freedom for the scalar unknown are located on the vertices of the mesh.

We also mention the papers [6,7], where local expressions for the diffusion flux has been derived in the context of finite volume scheme for the diffusion equation. In the same framework, Le Potier has derived a local flux approximation in [22,21] which is very similar to the MPFA symmetric method and to our method.

Finally, it seems that the diffusion scheme derived from the SOM has the best combination of ideal properties of any previous finite-difference scheme. The only drawback lies in the fact that there are both

cell-centered and face-centered unknowns. In this way, with a mesh composed of N triangular (quadrangular) cells one has asymptotically $2.5N$ ($3N$) unknowns. In addition, the treatment of the supplementary face-centered unknowns leads to a more complicated algorithm than usual when coupling the diffusion scheme with the hydrodynamics.

This disadvantage has motivated us to propose a new cell-centered scheme, which retains as well as possible the good properties of the SOM diffusion scheme.

The main feature of our new algorithm lies in introduction of two normal fluxes and two temperatures on each edge. A local variational formulation written for each cell corner provides the discretization of the normal fluxes. This discretization shows that the normal fluxes depend on the temperatures defined on the two edges impinging on a node and also on the corresponding cell-centered temperature. The continuity of both edge-temperatures and normal fluxes written for each edge surrounding the node leads to a local, symmetric positive definite linear system. Its resolution enables us to eliminate locally the edge-temperatures as functions of the cell-temperatures. In this way, we locally construct a discrete effective conductivity tensor related to each node. This nodal tensor is symmetric positive definite. Finally, by summing these local tensors over all nodes, we obtain a global linear system for the cell-centered unknowns. Let us notice that the nodal construction of our scheme is well adapted to unstructured meshes.

In summary, our new diffusion scheme has the following properties:

- It has only cell-centered unknowns.
- It has a local stencil.
- It has a symmetric positive definite representation for the diffusion operator.
- For triangular grids, it preserves linear solutions and gives the second order accuracy with or without material discontinuities.
- For rectangular grids, it reduces to the standard five-point scheme and the treatment of discontinuous conductivity coefficients is equivalent to the well known harmonic averaging procedure.
- For non-orthogonal grids, it gives an accuracy which is almost second order with or without material discontinuities.
- For non smooth quadrangular grids, it suffers the reduction or the loss of convergence.

It is interesting to note that our method, like the MPFA reference space method [5] suffers the reduction or the loss of convergence on quadrangular random grids i.e., the grids with perturbations of order h, where h is the mesh size parameter. However, such grids are seldom encountered in real life simulations. Moreover, we currently use our scheme in Arbitrary Lagrangian Eulerian (ALE) computations. In this context the rezoning procedure always produces a smooth mesh and we know that for such a mesh our scheme shows a second order convergence.

The remainder of this paper is organized as follows. We first give the problem statement and introduce the notations and assumptions. This is followed by the derivation of the diffusion operator discretization. We also provide the discretization of the Neumann and Dirichlet boundary conditions. We next present briefly the time discretization. Finally, computational results are given, followed by conclusions.

2. Problem statement, notations and assumptions

2.1. Problem statement

Let Ω be an open subset of $\mathbb{R}^2$ and $u \equiv u(x,y,t)$ be the solution of the following general diffusion problem:

$$\begin{aligned} &\rho C \frac{\partial u}{\partial t} - \nabla \cdot (D \nabla u) = S, (x,y) \in \Omega, \\ &u(x,y,0) = u^0(x,y). \end{aligned} \tag{1}$$

If u is homogeneous to a temperature, D is a scalar diffusion coefficient. ρ and C are respectively the density and the calorific capacity of the medium. S denotes a source term. The initial condition is denoted by u^0. We

denote by $\mathbf{\Phi} = -D\nabla u$, the diffusion flux. In this paper, we will study boundary conditions of the Dirichlet or Neumann type:

$$u = u_1, (x,y) \in \partial\Omega_1,$$
$$\mathbf{\Phi}\cdot\boldsymbol{N} = \Phi_2, (x,y) \in \partial\Omega_2,$$

where $\partial\Omega = \partial\Omega_1 \cup \partial\Omega_2$ and $\boldsymbol{N}$ denote the outward unit normal vector. The temperature imposed on $\partial\Omega_1$ is denoted by u_1 and Φ_2 denotes the normal flux imposed on $\partial\Omega_2$.

2.2. Notations and assumptions

The domain Ω is paved with a collection of non overlapping polygons: $\{\Omega_i, i = 1 \dots I\}$. Here, i denotes the index of cell Ω_i in the global numbering of cells and I is the total number of cells. A polygonal cell Ω_i is built with vertices labeled P_r see Fig. 1. Let $R(i)$ denote the number of vertices of Ω_i. We use a periodic counter clockwise numbering for the vertices, i.e. $P_{R(i)+1} = P_1$ and $P_0 = P_{R(i)}$. The length of the edge $[P_r, P_{r+1}]$ is denoted by $L_{r,r+1}$. The frame $(0,x,y)$ is equipped with an orthonormal basis $(\boldsymbol{e}_x, \boldsymbol{e}_y)$ which is completed with $\boldsymbol{e}_z = \boldsymbol{e}_x \times \boldsymbol{e}_y$. Let us denote by $P_{r+\frac{1}{2}}$ the midpoint of the edge $[P_r, P_{r+1}]$ and its outward unit normal by $\boldsymbol{N}_{r,r+1}$. We split the cell Ω_i into sub-cells Ω_r^i related to the vertex P_r. Ω_r^i is the quadrilateral whose vertices are $P_{r-\frac{1}{2}}$, P_r, $P_{r+\frac{1}{2}}$ and G_i where G_i is the centroid of Ω_i. With these notations, one can write:

$$\Omega_i = \bigcup_{r=1}^{R(i)} \Omega_r^i.$$

In order to build a discretization scheme for the diffusion equation, we define the discrete unknowns on cell Ω_i. First of all, let u_i be the mean value of u in the cell Ω_i :

$$u_i(t) = \frac{1}{V_i}\int_{\Omega_i} u(x,y,t)\,\mathrm{d}\Omega,$$

where V_i is the volume of Ω_i. Thus, the approximation space for the scalar variable u is made of piecewise constant functions.

We define in the same way the mean density ρ_i, the mean calorific capacity C_i and the source term S_i which are known quantities.

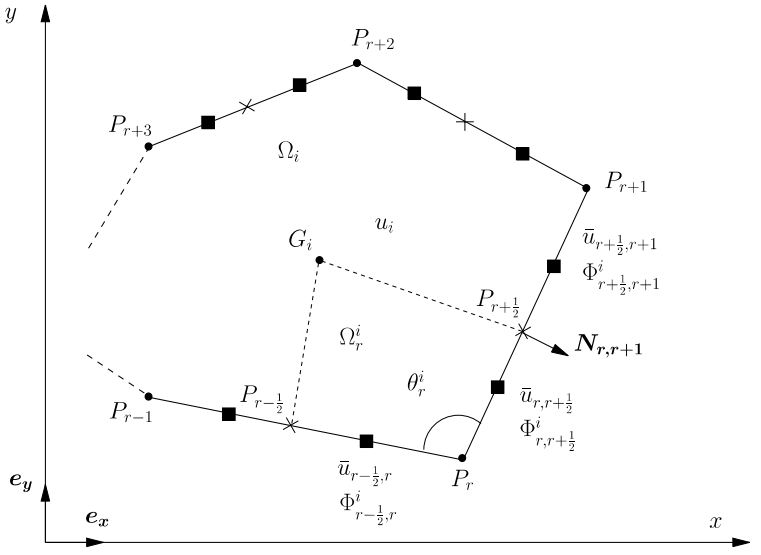

Fig. 1. Notations for cell Ω_i.

By integrating (1) over the cell Ω_i and using Green formula, one obtains

$$m_i C_i \frac{\mathrm{d}u_i}{\mathrm{d}t} + \int_{\partial\Omega_i} \mathbf{\Phi}\cdot\boldsymbol{N}\,\mathrm{d}l = V_i S_i,$$

where $m_i = \rho_i V_i$ is the mass of cell Ω_i, $\partial\Omega_i$ is the boundary of Ω_i and $\mathrm{d}l$ is the length element on $\partial\Omega_i$. Let $\Phi^i_{r,r+1}$ be the normal face flux on the edge $[P_r, P_{r+1}]$, it is defined by

$$L_{r,r+1}\Phi^i_{r,r+1} = \int_{P_r}^{P_{r+1}} \mathbf{\Phi}\cdot\boldsymbol{N}\,\mathrm{d}l. \tag{2}$$

We have added the superscript i in order to underline that the normal face flux is seen from cell Ω_i. Using this definition, we get

$$m_i C_i \frac{\mathrm{d}u_i}{\mathrm{d}t} + \sum_{r=1}^{R(i)} L_{r,r+1}\Phi^i_{r,r+1} = V_i S_i. \tag{3}$$

The main problem, as in all finite volume approaches, lies in the approximation of the normal face flux defined by (2). In order to design our approximation, we split the normal face flux $\Phi^i_{r,r+1}$ into the two normal face fluxes $\Phi^i_{r,r+\frac{1}{2}}$ and $\Phi^i_{r+\frac{1}{2},r+1}$ which are defined by

$$\begin{aligned} \frac{1}{2}L_{r,r+1}\Phi^i_{r,r+\frac{1}{2}} &= \int_{P_r}^{P_{r+\frac{1}{2}}} \mathbf{\Phi}\cdot\boldsymbol{N}\,\mathrm{d}l, \\ \frac{1}{2}L_{r,r+1}\Phi^i_{r+\frac{1}{2},r+1} &= \int_{P_{r+\frac{1}{2}}}^{P_{r+1}} \mathbf{\Phi}\cdot\boldsymbol{N}\,\mathrm{d}l. \end{aligned} \tag{4}$$

We immediately verify that

$$\Phi^i_{r,r+1} = \frac{1}{2}(\Phi^i_{r,r+\frac{1}{2}} + \Phi^i_{r+\frac{1}{2},r+1}).$$

Using this last result, we rewrite (3) as

$$m_i C_i \frac{\mathrm{d}u_i}{\mathrm{d}t} + \sum_{r=1}^{R(i)} \frac{1}{2}(L_{r-1,r}\Phi^i_{r-\frac{1}{2},r} + L_{r,r+1}\Phi^i_{r,r+\frac{1}{2}}) = V_i S_i. \tag{5}$$

We notice that this equation could have been obtained by integrating (1) over the sub-cell Ω^i_r, knowing that the flux across the sub-cells is zero.

We make the assumption that the trace of u is continuous across the edges of the cell Ω_i and we introduce $\bar{u}_{r,r+1}$ the face value of the temperature on the edge $[P_r, P_{r+1}]$

$$L_{r,r+1}\bar{u}_{r,r+1} = \int_{Pr}^{P_{r+1}} u\,\mathrm{d}l. \tag{6}$$

As it has been done for the face flux, we also define the two face values

$$\begin{aligned} \frac{1}{2}L_{r,r+1}\bar{u}_{r,r+\frac{1}{2}} &= \int_{Pr}^{P_{r+\frac{1}{2}}} u\,\mathrm{d}l, \\ \frac{1}{2}L_{r,r+1}\bar{u}_{r+\frac{1}{2},r+1} &= \int_{P_{r+\frac{1}{2}}}^{P_{r+1}} u\,\mathrm{d}l. \end{aligned} \tag{7}$$

we also have

$$\bar{u}_{r,r+1} = \frac{1}{2}(\bar{u}_{r,r+\frac{1}{2}} + \bar{u}_{r+\frac{1}{2},r+1}).$$

Thus, we assume that the scalar variable u is defined on each edge $[P_r, P_{r+1}]$ by the two constant values $\bar{u}_{r,r+\frac{1}{2}}$ and $\bar{u}_{r+\frac{1}{2},r+1}$.

We suppose that the diffusion coefficient is constant in each cell, and we denote by D_i its mean value in Ω_i.

We shall provide a discretization of the normal face fluxes from the face values. This is the topic of the next section.

3. Spatial discretization

3.1. Discretization of the diffusion flux

The main goal of this section is to provide a discretization of the diffusion flux $\mathbf{\Phi} = -D\nabla u$ using a local variational formulation. First, we introduce some preliminary results.

3.1.1. Preliminary results

We will show how to reconstruct a vector $\mathbf{\Psi}_r^i$ at each node of the cell Ω_i from its edge-normal components. Then, we will use this in order to define the dot product between two vectors $\mathbf{\Psi}_r^i$ and $\mathbf{\Phi}_r^i$. This result is classical and can be found in [18]. We recall its demonstration because it is the first step in order to build our spatial discretization for the diffusion equation.

Let $(\Psi_r^{ix}, \Psi_r^{iy})$ be the Cartesian coordinates of $\mathbf{\Psi}_r^i$ in the orthonormal basis $(\boldsymbol{e}_x, \boldsymbol{e}_y)$. From the definition of the edge-normal components the Cartesian coordinates of $\mathbf{\Psi}_r^i$ are solutions of the linear system

$$\begin{aligned}
&\Psi_r^{ix} N_{r-1,r}^x + \Psi_r^{iy} N_{r-1,r}^y = \Psi^i_{r-\frac{1}{2},r},\\
&\Psi_r^{ix} N_{r,r+1}^x + \Psi_r^{iy} N_{r,r+1}^y = \Psi^i_{r,r+\frac{1}{2}}.
\end{aligned}$$

The determinant of this linear system is $\Delta_r^i = N_{r-1,r}^x N_{r,r+1}^y - N_{r-1,r}^y N_{r,r+1}^x$. A simple calculation gives

$$\Delta_r^i = (\boldsymbol{N}_{r-1,r} \times \boldsymbol{N}_{r,r+1}) \cdot \boldsymbol{e_z} = \sin\theta_r^i,$$

where θ_r^i is the angle in Ω_i at vertex P_r, see Fig. 1. We make the assumption that $\Delta_r^i \neq 0$ and consequently, the linear system has always a unique solution. Introducing the matrix J_r^i:

$$\mathsf{J}_r^i = \frac{1}{\Delta_r^i}\begin{pmatrix} N_{r,r+1}^y & -N_{r-1,r}^y \\ -N_{r,r+1}^x & N_{r-1,r}^x \end{pmatrix},$$

one can write

$$\mathbf{\Psi}_r^i = \mathsf{J}_r^i \begin{pmatrix} \Psi^i_{r-\frac{1}{2},r} \\ \Psi^i_{r,r+\frac{1}{2}} \end{pmatrix}.$$

Then, it is straightforward to express the dot product between the two vectors $\mathbf{\Psi}_r^i$ and $\mathbf{\Phi}_r^i$ using their edge-normal components:

$$\langle \mathbf{\Psi}_r^i \cdot \mathbf{\Phi}_r^i \rangle = \mathsf{J}_r^i \begin{pmatrix} \Psi^i_{r-\frac{1}{2},r} \\ \Psi^i_{r,r+\frac{1}{2}} \end{pmatrix} \cdot \mathsf{J}_r^i \begin{pmatrix} \Phi^i_{r-\frac{1}{2},r} \\ \Phi^i_{r,r+\frac{1}{2}} \end{pmatrix}, = \left(\mathsf{J}_r^i\right)^t \mathsf{J}_r^i \begin{pmatrix} \Psi^i_{r-\frac{1}{2},r} \\ \Psi^i_{r,r+\frac{1}{2}} \end{pmatrix} \cdot \begin{pmatrix} \Phi^i_{r-\frac{1}{2},r} \\ \Phi^i_{r,r+\frac{1}{2}} \end{pmatrix},$$

where the superscript t denotes the transpose matrix. Introducing $\mathsf{T}_r^i = \left(\mathsf{J}_r^i\right)^t \mathsf{J}_r^i$, a simple calculation shows that

$$\mathsf{T}_r^i = \frac{1}{\sin^2\theta_r^i}\begin{pmatrix} 1 & \cos\theta_r^i \\ \cos\theta_r^i & 1 \end{pmatrix}. \tag{8}$$

T_r^i is the metric tensor associated with vertex P_r in the cell Ω_i. It is a symmetric positive definite tensor. We notice that it reduces to the unity tensor I of $\mathbb{R}^2$ if $\theta_r^i = \frac{\pi}{2}$. Finally, the dot product between the vectors $\mathbf{\Psi}_r^i$ and $\mathbf{\Phi}_r^i$ is given by

$$\langle \mathbf{\Psi}_r^i \cdot \mathbf{\Phi}_r^i \rangle = \mathsf{T}_r^i \begin{pmatrix} \Psi^i_{r-\frac{1}{2},r} \\ \Psi^i_{r,r+\frac{1}{2}} \end{pmatrix} \cdot \begin{pmatrix} \Phi^i_{r-\frac{1}{2},r} \\ \Phi^i_{r,r+\frac{1}{2}} \end{pmatrix}. \tag{9}$$

3.1.2. A local variational formulation

In order to derive our flux discretization, we introduce a local variational formulation. This methodology, known as the *Support Operators Method*, has been developed in [9,18]. However, instead of writing the variational formulation on the cell Ω_i as it is usually done, we will write it on the sub-cell Ω_r^i. In this way, we will obtain an explicit discretization of the normal face fluxes as function of the face values.

For any vector $\mathbf{\Psi} \in \mathbb{R}^2$ and scalar u, one has the following identity:

$$\nabla \cdot (u\mathbf{\Psi}) = u\nabla \cdot \mathbf{\Psi} + \mathbf{\Psi} \cdot \mathbf{\nabla} u, = u\nabla \cdot \mathbf{\Psi} - D^{-1}\mathbf{\Psi} \cdot \mathbf{\Phi},$$

where D^{-1} is the inverse of the diffusion coefficient. We notice that this identity is naturally related to the mixed formulation

$$\rho C \frac{\partial u}{\partial t} + \nabla \cdot \mathbf{\Phi} = S,$$
$$D^{-1}\mathbf{\Phi} + \mathbf{\nabla} u = \mathbf{0},$$

classicaly used in the context of MFEM [27].

We integrate this identity over the cell Ω_i, using Green formula, and obtain:

$$\int_{\Omega_i} D^{-1}\mathbf{\Psi} \cdot \mathbf{\Phi} \, \mathrm{d}\Omega = -\left[\int_{\partial\Omega_i} u\mathbf{\Psi} \cdot \boldsymbol{N} \, \mathrm{d}l - \int_{\Omega_i} u\nabla \cdot \mathbf{\Psi} \, \mathrm{d}\Omega\right]. \tag{10}$$

A sufficient condition in order to satisfy this identity is to satisfy it on each sub-cell Ω_r^i. Finally, one obtains the sufficient condition

$$\int_{\Omega_r^i} D^{-1}\mathbf{\Psi} \cdot \mathbf{\Phi} \, \mathrm{d}\Omega = -\left[\int_{\partial\Omega_r^i} u\mathbf{\Psi} \cdot \boldsymbol{N} \, \mathrm{d}l - \int_{\Omega_r^i} u\nabla \cdot \mathbf{\Psi} \, \mathrm{d}\Omega\right]. \tag{11}$$

This sub-cell variational formulation is the first step in order to obtain a discretization for the diffusion flux.

We first discretize the right-hand side using the mean value u_i, the face values $\bar{u}_{r-\frac{1}{2},r}$, $\bar{u}_{r,r+\frac{1}{2}}$ and the edge-normal components $\Psi^i_{r-\frac{1}{2},r}$, $\Psi^i_{r,r+\frac{1}{2}}$, see Fig. 2. With these notations, one obtains for the first integral

$$\int_{\partial\Omega_r^i} u\mathbf{\Psi} \cdot \boldsymbol{N} \, \mathrm{d}l = \frac{1}{2}(L_{r-1,r}\bar{u}_{r-\frac{1}{2},r}\Psi^i_{r-\frac{1}{2},r} + L_{r,r+1}\bar{u}_{r,r+\frac{1}{2}}\Psi^i_{r,r+\frac{1}{2}}) - \frac{1}{2}(L_{r-1,r}\boldsymbol{N}_{r-1,r} + L_{r,r+1}\boldsymbol{N}_{\boldsymbol{r},\boldsymbol{r+1}}) \cdot \mathbf{\Psi}_i u_i, \tag{12}$$

where $\mathbf{\Psi}_i$ denotes the mean value of the vector $\mathbf{\Psi}$ in the cell Ω_i. The second term on the right-hand side takes into account the contribution of the interior of the cell.

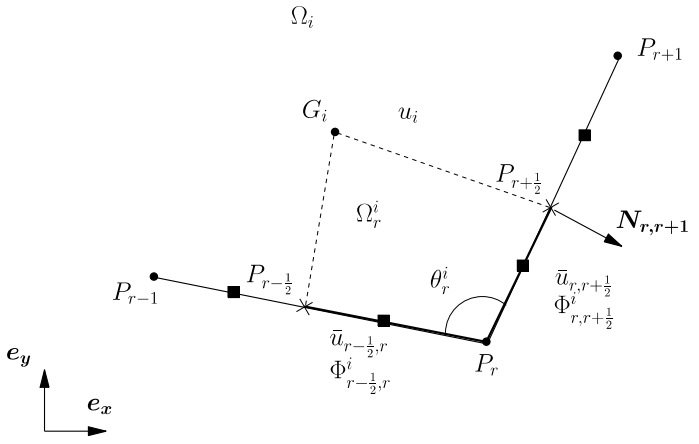

Fig. 2. Notations in the sub-cell Ω_r^i.

For the second integral we have

$$\int_{\Omega_r^i} u\nabla\cdot\boldsymbol{\Psi}\,\mathrm{d}\Omega = u_i\int_{\partial\Omega_r^i}\boldsymbol{\Psi}\cdot\boldsymbol{N}\,\mathrm{d}l = \frac{1}{2}\left(L_{r-1,r}\Psi^i_{r-\frac{1}{2},r}+L_{r,r+1}\Psi^i_{r,r+\frac{1}{2}}\right)u_i-\frac{1}{2}\left(L_{r-1,r}\boldsymbol{N}_{r-1,r}+L_{r,r+1}\boldsymbol{N}_{r,r+1}\right)\cdot\boldsymbol{\Psi}_i u_i. \tag{13}$$

Combining (12) and (13), we obtain:

$$\int_{\partial\Omega_r^i} u\boldsymbol{\Psi}\cdot\boldsymbol{N}\,\mathrm{d}l-\int_{\Omega_r^i}u\nabla\cdot\boldsymbol{\Psi}\,\mathrm{d}\Omega=\frac{1}{2}\left[L_{r-1,r}\Psi^i_{r-\frac{1}{2},r}\left(\bar{u}_{r-\frac{1}{2},r}-u_i\right)+L_{r,r+1}\Psi^i_{r,r+\frac{1}{2}}\left(\bar{u}_{r,r+\frac{1}{2}}-u_i\right)\right]. \tag{14}$$

Next, we approximate the left-hand side of (11) using the following quadrature:

$$\int_{\Omega_r^i} D^{-1}\boldsymbol{\Psi}\cdot\boldsymbol{\Phi}\,\mathrm{d}\Omega=\omega_r^i D_i^{-1}\langle\boldsymbol{\Psi}^i_r\cdot\boldsymbol{\Phi}^i_r\rangle,$$

where $\omega_r^i>0$ is a corner volume related to vertex P_r. This quadrature has to preserve constant function on cell Ω_i. Hence, the corner volumes must satisfy the following identity

$$\sum_{r=1}^{R(i)}\omega_r^i=V_i. \tag{15}$$

We notice that there are several possible choices for ω_r^i. The accuracy of the discretization is a consequence of these choices. We shall discuss some of them in Section 3.1.4.

Using (9), one can express the dot product between $\boldsymbol{\Psi}^i_r$ and $\boldsymbol{\Phi}^i_r$ in terms of their edge-normal components as follows:

$$\int_{\Omega_r^i} D^{-1}\boldsymbol{\Psi}\cdot\boldsymbol{\Phi}\,\mathrm{d}\Omega=\omega_r^i D_i^{-1}\mathsf{T}^i_r\begin{pmatrix}\Psi^i_{r-\frac{1}{2},r}\\ \Psi^i_{r,r+\frac{1}{2}}\end{pmatrix}\cdot\begin{pmatrix}\Phi^i_{r-\frac{1}{2},r}\\ \Phi^i_{r,r+\frac{1}{2}}\end{pmatrix}. \tag{16}$$

With (16) and (14) one can rewrite the expression of the local variational formulation:

$$\omega_r^i D_i^{-1}\mathsf{T}^i_r\begin{pmatrix}\Psi^i_{r-\frac{1}{2},r}\\ \Psi^i_{r,r+\frac{1}{2}}\end{pmatrix}\cdot\begin{pmatrix}\Phi^i_{r-\frac{1}{2},r}\\ \Phi^i_{r,r+\frac{1}{2}}\end{pmatrix}=-\frac{1}{2}\left[L_{r-1,r}\Psi^i_{r-\frac{1}{2},r}\left(\bar{u}_{r-\frac{1}{2},r}-u_i\right)+L_{r,r+1}\Psi^i_{r,r+\frac{1}{2}}\left(\bar{u}_{r,r+\frac{1}{2}}-u_i\right)\right]. \tag{17}$$

We recall that T^i_r is the metric tensor at vertex P_r in the cell Ω_i defined by (8). As the variational formulation (17) holds for any $\boldsymbol{\Psi}$, we first apply it for $\Psi^i_{r-\frac{1}{2},r}=1$, $\Psi^i_{r,r+\frac{1}{2}}=0$ and next for $\Psi^i_{r-\frac{1}{2},r}=0$, $\Psi^i_{r,r+\frac{1}{2}}=1$. Finally, one obtains:

$$\begin{pmatrix}\Phi^i_{r-\frac{1}{2},r}\\ \Phi^i_{r,r+\frac{1}{2}}\end{pmatrix}=-\frac{D_i}{2\omega_r^i}\left(\mathsf{T}^i_r\right)^{-1}\begin{bmatrix}L_{r-1,r}(\bar{u}_{r-\frac{1}{2},r}-u_i)\\ L_{r,r+1}(\bar{u}_{r,r+\frac{1}{2}}-u_i)\end{bmatrix}. \tag{18}$$

The computation of $\left(\mathsf{T}^i_r\right)^{-1}$ gives us:

$$\begin{pmatrix}\Phi^i_{r-\frac{1}{2},r}\\ \Phi^i_{r,r+\frac{1}{2}}\end{pmatrix}=-\frac{D_i}{2\omega_r^i}\begin{pmatrix}1 & -\cos\theta^i_r\\ -\cos\theta^i_r & 1\end{pmatrix}\begin{bmatrix}L_{r-1,r}(\bar{u}_{r-\frac{1}{2},r}-u_i)\\ L_{r,r+1}(\bar{u}_{r,r+\frac{1}{2}}-u_i)\end{bmatrix}. \tag{19}$$

We have obtained the discretization of the half normal fluxes. We point out that they depend on the metric tensor in the cell Ω_i at node P_r. They also depend on the half face values and the mean value.

3.1.3. Comparison with the discretization based on the SOM

We shall briefly recall the way the SOM provides the flux discretization, see [9,18].

Keeping the notations defined previously, one begins to write the following variational formulation in the cell Ω_i

$$\int_{\Omega_i} D^{-1}\boldsymbol{\Psi}\cdot\boldsymbol{\Phi}\,\mathrm{d}\Omega=-\left[\int_{\partial\Omega_i}u\boldsymbol{\Psi}\cdot\boldsymbol{N}\,\mathrm{d}l-\int_{\Omega_i}u\nabla\cdot\boldsymbol{\Psi}\,\mathrm{d}\Omega\right].$$

The discretization of this formulation is made using the face and the cell centered unknowns $\bar{u}_{r,r+1}$, u_i. The vectors $\mathbf{\Psi}$ and $\mathbf{\Phi}$ are expressed in terms of their edge-normal components $\Psi^i_{r,r+1}$, $\Phi^i_{r,r+1}$. After discretization of the right-hand side, one obtains:

$$\int_{\partial\Omega_i} u\mathbf{\Psi}\cdot\boldsymbol{N}\,\mathrm{d}l - \int_{\Omega_i} u\nabla\cdot\mathbf{\Psi}\,\mathrm{d}\Omega = \sum_{r=1}^{R(i)} L_{r,r+1}\Psi_{r,r+1}(\bar{u}_{r,r+1}-u_i),$$

where the sum is performed over all edges. For the left-hand side, one uses the following nodes quadrature formula:

$$\int_{\Omega_i} D^{-1}\mathbf{\Psi}\cdot\mathbf{\Phi}\,\mathrm{d}\Omega = \sum_{r=1}^{R(i)} \omega^i_r D_i^{-1}\langle\mathbf{\Psi}^i_r\cdot\mathbf{\Phi}^i_r\rangle,$$

where the sum is performed over all nodes. Introducing the expression of the dot product, one obtains:

$$\sum_{r=1}^{R(i)} \frac{\omega^i_r}{\sin^2\theta^i_r} D_i^{-1}\begin{pmatrix}1 & \cos\theta^i_r\\ \cos\theta^i_r & 1\end{pmatrix}\begin{pmatrix}\Psi^i_{r-1,r}\\ \Psi^i_{r,r+1}\end{pmatrix}\cdot\begin{pmatrix}\Phi^i_{r-1,r}\\ \Phi^i_{r,r+1}\end{pmatrix} = -\sum_{r=1}^{R(i)}[L_{r,r+1}\Psi^i_{r,r+1}(\bar{u}_{r,r+1}-u_i)].$$

This equation holds for any $\mathbf{\Psi}$, therefore one applies it for $\Psi^i_{r,r+1}=1$ and $\Psi^i_{k,k+1}=0$ with $k\neq r$. Hence, the normal components of the flux are the solution of a linear system whose rth row is given by

$$\frac{\omega^i_r}{\sin^2\theta^i_r}(\cos\theta^i_r\Phi^i_{r-1,r}+\Phi^i_{r,r+1}) + \frac{\omega^i_{r+1}}{\sin^2\theta^i_{r+1}}(\Phi^i_{r,r+1}+\cos\theta^i_{r+1}\Phi^i_{r+1,r+2}) = -D_iL_{r,r+1}(\bar{u}_{r,r+1}-u_i). \tag{20}$$

This equation shows that the normal components on the three consecutive edges $[P_{r-1},P_r]$, $[P_r,P_{r+1}]$ and $[P_{r+1},P_{r+2}]$ are strongly coupled. For instance, in the quadrangular mesh case, one obtains four coupled linear equations for the flux components, for details see [18]. Unfortunately, one cannot give explicit expressions for the flux components. Consequently, one has to deal with both cell u_i and face $\bar{u}_{r,r+1}$ centered unknowns, when solving the global diffusion problem.

In our formulation, thanks to the splitting of the cell Ω_i into sub-cells Ω^i_r, we have written a variational formulation which is local at node P_r, see Eq. (17). Hence, we are able to give explicitly the half normal fluxes $\Phi^i_{r-\frac{1}{2},r}$, $\Phi^i_{r,r+\frac{1}{2}}$ in terms of the half face values $\bar{u}_{r-\frac{1}{2},r}$, $\bar{u}_{r,r+\frac{1}{2}}$, see Eq. (19). We shall show in the next section that we are able to eliminate the face values by writing the continuity of the normal flux on all the edges which impinge on node P_r.

3.1.4. Evaluation of the corner volumes

3.1.4.1. For triangular cells. In [16], the authors perform a detailed analysis of the SOM for triangular cells. They show that their scheme preserves the linear solutions provided the corner volumes are equal to the third of the cell area.

With our method, by making the same choice we also obtain the same result. Namely, if for each triangular cell we set

$$\omega^i_r = \frac{1}{3}V_i,$$

then, we can show that our scheme preserves the linear solutions. The proof is straightforward and uses a finite element formalism. Let T be a generic triangular cell whose vertices are denoted by P_1, P_2 and P_3, see Fig. 3. We denote its area by V_T. We consider the classical P^1 basis on T defined by the three functions λ_1, λ_2 and λ_3. We recall that $\lambda_r\equiv\lambda_r(x,y)$, $r=1\ldots3$ is a linear function. The three basis functions are characterized by

$$\lambda_r(P_s)=0,\quad r\neq s$$
$$\lambda_r(P_r)=1.$$

In addition, we have $\lambda_1+\lambda_2+\lambda_3=1$. The field u is projected onto T by setting

$$u=\lambda_1u_1+\lambda_2u_2+\lambda_3u_3, \tag{21}$$

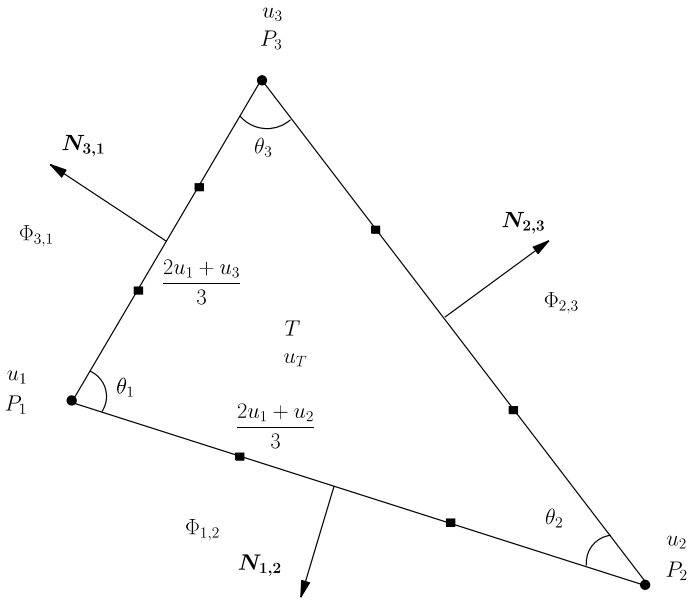

Fig. 3. Notations for triangular cell T.

where u_1, u_2 and u_3 denotes the nodal values of u. We notice that (21) is exact for the linear fields. Using this representation, we compute the normal components of the flux on each face of T. Let $\Phi_{r,r+1}$ be the normal component of $\mathbf{\Phi} = -D\nabla u$ on the face $[P_r, P_{r+1}]$. The diffusion coefficient on T is denoted by D_T. Knowing that

$$\nabla\lambda_r = \frac{1}{2V_T}(L_{r-1,r}\boldsymbol{N}_{r-1,r} + L_{r,r+1}\boldsymbol{N}_{\boldsymbol{r,r+1}}), \quad r = 1\ldots 3, \tag{22}$$

we obtain

$$\begin{aligned}\Phi_{1,2} &= -D_T\nabla u\cdot\boldsymbol{N}_{1,2}\\ &= -\frac{D_T}{2V_T}[(L_{1,2}-L_{3,1}\cos\theta_1)u_1 + (L_{1,2}-L_{2,3}\cos\theta_2)u_2 - (L_{2,3}\cos\theta_2 + L_{3,1}\cos\theta_1)u_3]\\ &= -\frac{D_T}{2V_T}[L_{1,2}(u_1+u_2) - L_{2,3}\cos\theta_2(u_2+u_3) - L_{3,1}\cos\theta_1(u_1+u_3)].\end{aligned} \tag{23}$$

If u is a constant field then $\Phi_{1,2} = 0$ and we have the following geometrical identity:

$$L_{1,2} - L_{2,3}\cos\theta_2 - L_{3,1}\cos\theta_1 = 0. \tag{24}$$

The same identity holds also for the edges $[P_2, P_3]$ and $[P_3, P_1]$. Combining (24) with (23) we get

$$\Phi_{1,2} = -\frac{D_T}{2V_T}[L_{1,2}(u_1-u_3) - L_{3,1}\cos\theta_1(u_1-u_2)]. \tag{25}$$

Now, in order to eliminate the nodal values we introduce the mean value of u over T

$$u_T = \frac{1}{3}(u_1+u_2+u_3).$$

We finally obtain

$$\Phi_{1,2} = -\frac{3D_T}{2V_T}\left[L_{1,2}\left(\frac{2u_1+u_2}{3} - u_T\right) - L_{3,1}\cos\theta_1\left(\frac{2u_1+u_3}{3} - u_T\right)\right]. \tag{26}$$

Following the same way, we also compute $\Phi_{3,1}$ and get

$$\Phi_{3,1} = -\frac{3D_T}{2V_T}\left[-L_{1,2}\cos\theta_1\left(\frac{2u_1+u_2}{3}-u_T\right)+L_{3,1}\left(\frac{2u_1+u_3}{3}-u_T\right)\right]. \tag{27}$$

Finally, (26) and (27) are rewritten in a more concise way

$$\begin{pmatrix}\Phi_{3,1}\\ \Phi_{1,2}\end{pmatrix} = -\frac{3D_T}{2V_T}\begin{pmatrix}1 & -\cos\theta_1\\ -\cos\theta_1 & 1\end{pmatrix}\begin{pmatrix}\frac{2u_1+u_3}{3}-u_T\\ \frac{2u_1+u_2}{3}-u_T\end{pmatrix}. \tag{28}$$

We point out that (28) gives an approximation of the normal components which is exact for linear functions. The comparison with (19) shows that with the choice $\omega_r^i = \frac{1}{3}V_i$, our scheme preserves linear solutions. In addition, it gives an interesting interpretation of the half face values $\bar{u}_{r-\frac{1}{2},r}$, $\bar{u}_{r,r+\frac{1}{2}}$ in terms of the nodal values, namely

$$\bar{u}_{r-\frac{1}{2},r} = \frac{2u_r+u_{r-1}}{3},$$
$$\bar{u}_{r,r+\frac{1}{2}} = \frac{2u_r+u_{r+1}}{3}.$$

3.1.4.2. For quadrangular cells. In [9], the authors develop the SOM for quadrilateral cells and they suggest to use a corner volume equal to the half of the area of the triangle formed by the vertices P_{r-1}, P_r and P_{r+1}, see Fig. 1. The numerical experiments in [9] show that this choice allows to preserve the linear solutions.

In the case of our method, we also make the same choice and we set for each quadrangular cell

$$\omega_r^i = \frac{1}{4}L_{r-1,r}L_{r,r+1}\sin\theta_r^i.$$

We will show in the section devoted to numerical results that this choice leads to a scheme which generally does not preserve the linear solution, unless the cells are parallelograms.

3.2. Elimination of the face values

In order to compute the edge values $\bar{u}_{r-\frac{1}{2},r}$ and $\bar{u}_{r,r+\frac{1}{2}}$ one writes the continuity of the normal flux across all the edges which impinge on node P_r. We choose an internal vertex P_q for $q = 1 \ldots Q_i$, i.e. $P_q \notin \partial\Omega$. The index q is a generic index in the global numbering of internal nodes and Q_i denotes the number of internal nodes. The case of the boundary vertex will be investigated in the section related to boundaries conditions.

3.2.1. Linear system satisfied by the face values

We introduce some new notations. The node P_q (see Fig. 4) is surrounded by cells Ω_k with $k = 1 \ldots K(q)$, where $K = K(q)$ is the number of cells around P_q. We use a periodic numbering for the cells. Notice that k is a generic index in the local numbering of the cells around node P_q. The cell Ω_k is enclosed by the two edges $[P_q, P_k]$ and $[P_q, P_{k+1}]$. The length of these edges are L_k and L_{k+1}. The angle made by these edges connected to node P_q is denoted θ_k. We denote by $P_{k+\frac{1}{2}}$ the midpoint of $[P_q, P_{k+1}]$.

We make the following assumptions:

- the scalar variable u is constant over the cell Ω_k and its value is denoted by u_k,
- we suppose that u is constant on each half edge $[P_q, P_{k+\frac{1}{2}}]$ and we denote its value by $\bar{u}_k$.

D_k denotes the constant value of the diffusion coefficient in the cell Ω_k. The corner volume related to node P_q is labeled ω_k. Finally, we denote by Φ_k^k the edge-normal component on the kth edge seen from the kth cell and by Φ_k^{k-1} the edge-normal component on the kth edge seen from the $(k-1)$th cell. These two fluxes are related to the half edge k connected to vertex P_q. With these notations, we can rewrite (19)

$$\begin{pmatrix}\Phi_k^k\\ \Phi_{k+1}^k\end{pmatrix} = -\frac{D_k}{2\omega_k}\begin{pmatrix}1 & -\cos\theta_k\\ -\cos\theta_k & 1\end{pmatrix}\begin{bmatrix}L_k(\bar{u}_k-u_k)\\ L_{k+1}(\bar{u}_{k+1}-u_k)\end{bmatrix}. \tag{29}$$

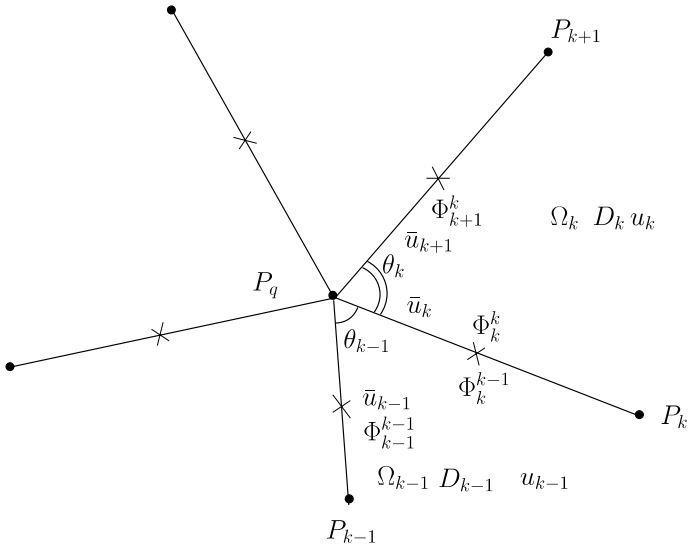

Fig. 4. Notations around an internal vertex P_q.

In order to obtain the expression of Φ_k^{k-1} one writes the analogous of (29) for the $(k-1)$th cell

$$\Phi_k^{k-1} = -\frac{1}{2}\alpha_{k-1}[-\cos\theta_{k-1}L_{k-1}(\bar{u}_{k-1} - u_{k-1}) + L_k(\bar{u}_k - u_{k-1})],$$
$$\Phi_k^k = -\frac{1}{2}\alpha_k[L_k(\bar{u}_k - u_k) - \cos\theta_k L_{k+1}(\bar{u}_{k+1} - u_k)],$$

where $\alpha_k = \frac{D_k}{\omega_k}$ is assumed to be a real and non negative number.

The continuity of the normal flux across the kth edge is written

$$\frac{1}{2}L_k\left(\Phi_k^{k-1} + \Phi_k^k\right) = 0. \tag{30}$$

This continuity condition provides us K equations for the K unknowns $\bar{u}_k$. We substitute the expressions of Φ_k^{k-1} and Φ_k^k into (30). Then, one obtains a linear system of K equations for the unknowns $\bar{u}_k$. After some algebra, one gets the kth row of this system

$$\begin{aligned}&-\alpha_{k-1}\cos\theta_{k-1}L_{k-1}L_k\bar{u}_{k-1} + (\alpha_{k-1} + \alpha_k)L_k^2\bar{u}_k - \alpha_k\cos\theta_k L_k L_{k+1}\bar{u}_{k+1}\\ &\quad = \alpha_{k-1}L_k(L_k - L_{k-1}\cos\theta_{k-1})u_{k-1} + \alpha_k L_k(L_k - L_{k+1}\cos\theta_{k+1})u_k.\end{aligned} \tag{31}$$

The matrix associated with this linear system is denoted by M. This is a $K\times K$ sparse matrix. The non zero terms are detailed below:

- First row:

$$\mathsf{M}_{1,1} = (\alpha_1 + \alpha_K)L_1^2,$$
$$\mathsf{M}_{1,2} = -\alpha_1\cos\theta_1 L_1 L_2,$$
$$\mathsf{M}_{1,K} = -\alpha_K L_K L_1\cos\theta_K,$$

- kth row:

$$\mathsf{M}_{k,k-1} = -\alpha_{k-1}\cos\theta_{k-1}L_{k-1}L_k,$$
$$\mathsf{M}_{k,k} = (\alpha_{k-1} + \alpha_k)L_k^2,$$
$$\mathsf{M}_{k,k+1} = -\alpha_k\cos\theta_k L_k L_{k+1},$$

- Kth row:

$$\begin{aligned}
&\mathsf{M}_{K,1} = -\alpha_K \cos\theta_K L_K L_1,\\
&\mathsf{M}_{K,K-1} = -\alpha_{K-1} \cos\theta_{K-1} L_{K-1} L_K,\\
&\mathsf{M}_{K,K} = (\alpha_{K-1} + \alpha_K) L_K^2.
\end{aligned}$$

It is clear that M is a symmetric matrix. Moreover, it admits the following decomposition

$$\mathsf{M} = \mathsf{LNL}. \tag{32}$$

The matrix L is a diagonal matrix defined by $\mathsf{L}_{k,l} = L_k \delta_{k,l}$ where $\delta_{k,l}$ is the Kronecker symbol, i.e. if $k = l$ then $\delta_{k,l} = 1$, otherwise $\delta_{k,l} = 0$. The matrix N is a $K \times K$ symmetric matrix, its kth row is given by

$$\begin{aligned}
&\mathsf{N}_{k,k-1} = -\alpha_{k-1} \cos\theta_{k-1},\\
&\mathsf{N}_{k,k} = (\alpha_{k-1} + \alpha_k),\\
&\mathsf{N}_{k,k+1} = -\alpha_k \cos\theta_k.
\end{aligned}$$

Note that $\alpha_k > 0$ therefore, N is diagonally dominant. Moreover, $\mathsf{N}_{k,k} > 0$ hence N is a symmetric positive definite matrix. Finally, M is also symmetric positive definite and the linear system for the face values $\bar{u}_k$ has always a unique solution.

Comment 1. If for any $k = 1 \ldots K$ we have $\theta_k \in [-\frac{\pi}{2}, \frac{\pi}{2}]$ then M is an M-matrix. The proof is straightforward since with the previous angular conditions we have $\mathsf{M}_{k,l} \leqslant 0$ for $k \neq l$.

The right-hand side of (31) can be put in a more concise form. Let S be a $K \times K$ sparse matrix S whose non zero terms of its kth row are defined by

$$\begin{aligned}
&\mathsf{S}_{k,k-1} = \alpha_{k-1} L_k (L_{k-L_{k-1}} \cos\theta_{k-1}),\\
&\mathsf{S}_{k,k} = \alpha_k L_k (L_{k-L_{k+1}} \cos\theta_k),
\end{aligned} \tag{33}$$

for $k = 1 \ldots K$, using periodicity.

Let us introduce the two vectors of $\mathbb{R}^K$ defined by: $\bar{\boldsymbol{U}} = (\bar{u}_1 \ldots \bar{u}_K)^t$ and $\boldsymbol{U} = (u_1 \ldots u_K)^t$. Then, the linear system (31) reduces to

$$\mathsf{M}\bar{\boldsymbol{U}} = \mathsf{S}\boldsymbol{U}. \tag{34}$$

This system always admits a unique solution, therefore one can compute the face unknowns $\bar{u}_k$ from the mean values u_k and the geometry around the vertex P_q. At this stage, let us remark that the face value on the kth edge depends on all the mean values u_k around the vertex P_q since M^{-1} is a full matrix.

Comment 2. If the mean values around P_q are non negative, the positivity of the face values is guaranteed under the following geometric conditions:

$$\begin{aligned}
&\theta_k \in \left[-\frac{\pi}{2}, \frac{\pi}{2}\right], \quad \forall\, k = 1 \ldots K,\\
&\cos\theta_k \leqslant \min\left(\frac{L_k}{L_{k+1}}, \frac{L_{k+1}}{L_k}\right).
\end{aligned} \tag{35}$$

The first condition implies that M is an M-matrix, and the second $\mathsf{S}_{k,l} \geqslant 0$. Consequently $\mathsf{F} = \mathsf{M}^{-1}\mathsf{S}$ is such that $\mathsf{F}_{k,l} \geqslant 0$. In this way, if $u_k \geqslant 0$ then $\bar{u}_k \geqslant 0$. Note that the geometric conditions (35) are very restrictive and could be violated with distorted grids. However, it will be a useful criterion in order to detect the effect of mesh distortion on our scheme.

3.2.2. Case of a rectangular mesh

Let us investigate the special case corresponding to $K = 4$ with $\theta_k = \frac{\pi}{2}$. In this case, four rectangular cells surround the vertex P_q, see Fig. 5. The matrix M is diagonal

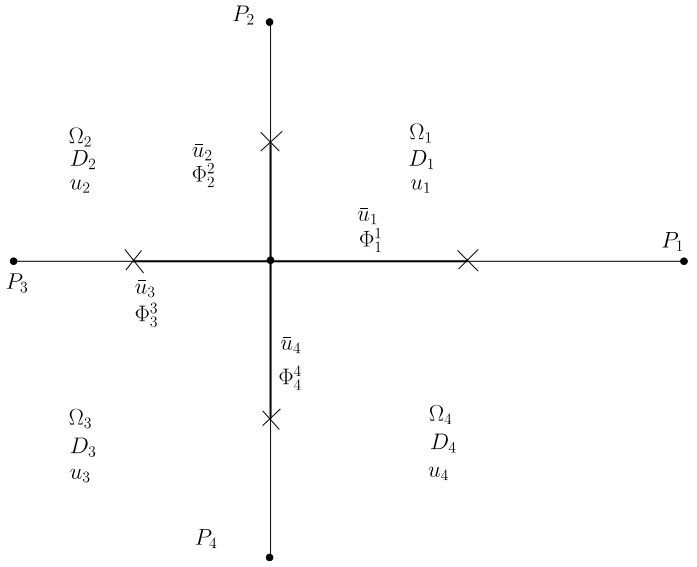

Fig. 5. Special case of rectangular cells.

$$\mathsf{M} = \begin{pmatrix} (\alpha_4+\alpha_1)L_1^2 & 0 & 0 & 0 \\ 0 & (\alpha_1+\alpha_2)L_2^2 & 0 & 0 \\ 0 & 0 & (\alpha_2+\alpha_3)L_3^2 & 0 \\ 0 & 0 & 0 & (\alpha_3+\alpha_4)L_4^2 \end{pmatrix},$$

and the matrix S is given by

$$\mathsf{S} = \begin{pmatrix} \alpha_1 L_1^2 & 0 & 0 & \alpha_4 L_1^2 \\ \alpha_1 L_2^2 & \alpha_2 L_2^2 & 0 & 0 \\ 0 & \alpha_2 L_3^2 & \alpha_3 L_3^2 & 0 \\ 0 & 0 & \alpha_3 L_4^2 & \alpha_4 L_4^2 \end{pmatrix}.$$

The computation of $\bar{\boldsymbol{U}} = \mathsf{M}^{-1}\mathsf{S}\boldsymbol{U}$ is straightforward and it provides

$$\bar{u}_k = \frac{\alpha_{k-1}u_{k-1} + \alpha_k u_k}{\alpha_{k-1} + \alpha_k},$$

where $k = 1 \ldots 4$ with periodicity ($u_0 = u_4$ and $\alpha_0 = \alpha_4$). Substituting face values in (29), we compute the flux on the four edges using $\omega_k = \frac{1}{4}L_k L_{k+1}$ for $k = 1 \ldots 4$ with periodicity

$$\boldsymbol{\Phi}_k^k = -\frac{2}{\frac{L_{k-1}}{D_{k-1}} + \frac{L_{k+1}}{D_k}}(u_{k-1} - u_k).$$

We recover the classical interpolation for the face values which is used in order to get an harmonic averaging for the conductivity on the interfaces. In the case of a rectangular mesh, our formulation reduces to the classical five-point scheme.

3.2.3. Property of the matrix F

Before ending this section, we shall give a useful property concerning the matrix $\mathsf{F} = \mathsf{M}^{-1}\mathsf{S}$. The matrix F enables us to express the face values: $\bar{\boldsymbol{U}} = \mathsf{F}\boldsymbol{U}$. This matrix satisfies the following property:

$$\forall\ k = 1 \ldots K \quad \sum_{l=1}^{K} \mathsf{F}_{k,l} = 1. \tag{36}$$

The proof is straightforward. First, let us notice that $\forall\ k = 1 \dots K$:

$$\sum_{l=1}^{K} \mathsf{M}_{k,l} = \sum_{l=1}^{K} \mathsf{S}_{k,l}. \tag{37}$$

Next, we consider a uniform field of mean values $\boldsymbol{U}^\star = u^\star(1 \dots 1)^t$ surrounding the node P_q where $u^\star$ is a constant value. One computes the face values vector $\bar{\boldsymbol{U}}$, solution of $\mathsf{M}\bar{\boldsymbol{U}} = \mathsf{S}\boldsymbol{U}^\star$. The kth component of $\mathsf{S}\boldsymbol{U}^\star$ is given by

$$\begin{aligned}
(\mathsf{S}\boldsymbol{U}^\star)_k &= \sum_{l=1}^{K} \mathsf{S}_{k,l} U_l^\star, \\
&= u^\star \sum_{l=1}^{K} \mathsf{S}_{k,l}, \\
&= u^\star \sum_{l=1}^{K} \mathsf{M}_{k,l}, \quad \text{using (37)} \\
&= (\mathsf{M}\boldsymbol{U}^\star)_k.
\end{aligned}$$

This implies that $\mathsf{M}\bar{\boldsymbol{U}} = \mathsf{M}\boldsymbol{U}^\star$ and therefore, $\bar{\boldsymbol{U}} = \boldsymbol{U}^\star$. Then, face values are also constant and equal to $u^\star$. Finally, one obtains $\boldsymbol{U}^\star = \mathsf{F}\boldsymbol{U}^\star$ and the announced result.

As a conclusion, let us emphasize that we are able to eliminate the face values $\bar{\boldsymbol{U}}$ solving the linear system $\mathsf{M}\bar{\boldsymbol{U}} = \mathsf{S}\boldsymbol{U}$, whatever the number of cells surrounding the vertex P_q. Moreover, M is a symmetric positive definite matrix. This property will be useful when we construct the global diffusion matrix.

3.3. Construction of the diffusion matrix at internal vertices

In this section, we will use the elimination of the face values in order to construct a cell-centered discretization for the diffusion equation. We recall the semi-discretized equation satisfied by the cell-centered unknown u_i

$$m_i \frac{\mathrm{d}u_i}{\mathrm{d}t} + \sum_{r=1}^{R(i)} \frac{1}{2} \left(L_{r-1,r} \Phi^i_{r-\frac{1}{2},r} + L_{r,r+1} \Phi^i_{r,r+\frac{1}{2}} \right) = V_i S_i. \tag{38}$$

3.3.1. Computation of the node contribution to diffusion flux

Our purpose, is to express the node contribution to the diffusion flux in cell Ω_i, that is to evaluate

$$\frac{1}{2} \left(L_{r-1,r} \Phi^i_{r-\frac{1}{2},r} + L_{r,r+1} \Phi^i_{r,r+\frac{1}{2}} \right).$$

We perform this evaluation for an internal node, i.e. $P_r \notin \partial\Omega$. The case of boundary nodes will be developed in the next section.

We denote by q the global index of node P_r in the global numbering of nodes. Hence $P_r \equiv P_q$ is surrounded by $K(q)$ cells, see Fig. 6. Let $k \equiv k(i)$ be the local index of cell Ω_i in the local numbering around node P_q. We recall that the local numbering of cells around node P_q is periodic. Here, we use the notations which have been defined in the last section. With these local notations, we have $u_i \equiv u_k$, $L_{r-1,r} \equiv L_{k+1}$, $L_{r,r+1} \equiv L_k$, $\bar{u}_{r-\frac{1}{2},r} \equiv \bar{u}_{k+1}$, $\bar{u}_{r,r+\frac{1}{2}} \equiv \bar{u}_k$, $\Phi^i_{r-\frac{1}{2},r} \equiv \Phi^k_{k+1}$ and $\Phi^i_{r,r+\frac{1}{2}} \equiv \Phi^k_k$. We also define $\alpha_k = \frac{D_i}{\omega^i_r}$ where D_i denotes the conductivity in cell Ω_i and ω^i_r the corner volume related to vertex P_r in cell Ω_i. Finally, node P_q contribution to the flux in cell Ω_i is

$$C_k = \frac{1}{2} \left(L_k \Phi^k_k + L_{k+1} \Phi^k_{k+1} \right). \tag{39}$$

We evaluate this contribution using (29)

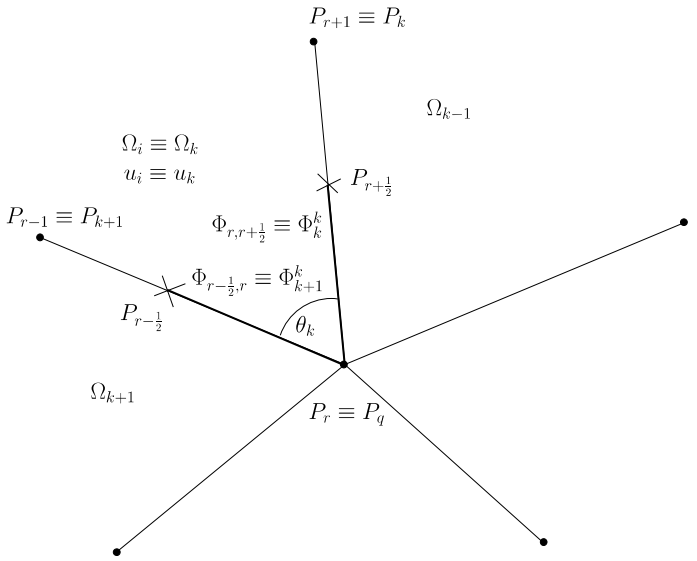

Fig. 6. Local numbering around an internal node P_q.

$$\begin{pmatrix} \Phi_k^k \\ \Phi_{k+1}^k \end{pmatrix} = -\frac{\alpha_k}{2} \begin{pmatrix} 1 & -\cos\theta_k \\ -\cos\theta_k & 1 \end{pmatrix} \begin{bmatrix} L_k(\bar{u}_k - u_k) \\ L_{k+1}(\bar{u}_{k+1} - u_k) \end{bmatrix}. \tag{40}$$

We recall that the face values are expressed in terms of mean values using matrices M and S as follows: $\bar{\boldsymbol{U}} = \mathsf{M}^{-1}\mathsf{S}\boldsymbol{U} = \mathsf{F}\boldsymbol{U}$. Hence, $\bar{u}_k$ and $\bar{u}_{k+1}$ are given by

$$\bar{u}_k = \sum_{l=1}^{K} \mathsf{F}_{k,l} u_l,$$
$$\bar{u}_{k+1} = \sum_{l=1}^{K} \mathsf{F}_{k+1,l} u_l,$$

where F is a matrix which depends on the geometry and the diffusion coefficients around vertex P_q.

In order to compute C_k, we substitute the expressions of Φ_k^k and Φ_{k+1}^k from (40) into (39). Then, one obtains:

$$C_k = -\frac{\alpha_k}{4}[L_k(L_k - L_{k+1}\cos\theta_k)(\bar{u}_k - u_k) + L_{k+1}(L_{k+1} - L_k\cos\theta_k)(\bar{u}_{k+1} - u_k)]. \tag{41}$$

On the right-hand side of (41) we identify $\mathsf{S}_{k,k} = \alpha_k L_k(L_k - L_{k+1}\cos\theta_k)$ and $\mathsf{S}_{k+1,k} = \alpha_k L_{k+1}(L_{k+1} - L_k\cos\theta_k)$. These two terms correspond to the kth column of matrix S defined by (33). Since the other terms of the kth column of S are zero, one can rewrite C_k as follows:

$$C_k = -\frac{1}{4}\left[\sum_{l=1}^{K} \mathsf{S}_{l,k}(\bar{u}_l - u_l)\right].$$

In order to recover a matrix vector product in the previous equation, one introduces the transpose of S

$$C_k = -\frac{1}{4}\left[\sum_{l=1}^{K} \mathsf{S}_{k,l}^t(\bar{u}_l - u_l)\right]. \tag{42}$$

A simple calculation shows that

$$\sum_{l=1}^{K} \mathsf{S}_{k,l}^t = \mathsf{S}_{k,k} + \mathsf{S}_{k+1,k}, = \alpha_k(L_k^2 + L_{k+1}^2 - 2L_kL_{k+1}\cos\theta_k) > 0,$$

since $\alpha_k > 0$. The term between the brackets has a simple geometric interpretation. Its square root is the length of the edge joining the vertices P_{r-1} and P_{r+1}, see Fig. 6. We denote it by λ_k

$$\lambda_k^2 = L_k^2 + L_{k+1}^2 - 2L_kL_{k+1}\cos\theta_k.$$

Finally, we introduce a diagonal matrix Λ defined by

$$\Lambda_{k,l} = \alpha_k\lambda_k^2\delta_{k,l}. \tag{43}$$

With these new notations and recalling that $\bar{\boldsymbol{U}} = \mathsf{M}^{-1}\mathsf{S}\boldsymbol{U}$, we rewrite (42)

$$\boldsymbol{C} = -\frac{1}{4}(\mathsf{S}^t\mathsf{M}^{-1}\mathsf{S} - \Lambda)\boldsymbol{U}, \tag{44}$$

where $\boldsymbol{C}$ is the flux contribution vector defined by: $\boldsymbol{C} = (C_1 \dots C_K)^t$. In order to clarify this last result, we introduce

$$\Gamma = -\frac{1}{4}(\mathsf{S}^t\mathsf{M}^{-1}\mathsf{S} - \Lambda).$$

Γ is also a $K \times K$ symmetric matrix. It verifies the important property

$$\forall\ k = 1 \dots K \quad \sum_{l=1}^{K}\Gamma_{k,l} = 0. \tag{45}$$

This property involves the conservativity of the diffusion scheme. If the mean values around node P_q are uniform and equal to $u^\star$, i.e. $\boldsymbol{U} = \boldsymbol{U}^\star = u^\star(1 \dots 1)^t$, then, with (45), $\Gamma\boldsymbol{U}^\star = \boldsymbol{0}$ therefore, $\boldsymbol{C} = \boldsymbol{0}$ and the diffusion fluxes around P_q are zero. The proof of this property is based on the property (36) satisfied by the matrix $\mathsf{F} = \mathsf{M}^{-1}\,\mathsf{S}$. Knowing that $\Gamma = \mathsf{S}^t\mathsf{F}$ we get

$$\Gamma_{k,l} = -\frac{1}{4}\left(\sum_{m=1}^{K}\mathsf{S}_{k,m}^t\mathsf{F}_{m,l} - \Lambda_{k,l}\right).$$

Summing over l gives

$$\begin{aligned}
\sum_{l=1}^{K}\Gamma_{k,l} &= -\frac{1}{4}\left(\sum_{l=1}^{K}\sum_{m=1}^{K}\mathsf{S}_{k,m}^t\mathsf{F}_{m,l} - \Lambda_{k,k}\right),\\
&= -\frac{1}{4}\left(\sum_{m=1}^{K}\mathsf{S}_{k,m}^t\sum_{l=1}^{K}\mathsf{F}_{m,l} - \sum_{l=1}^{K}\mathsf{S}_{k,l}^t\right),\\
&= -\frac{1}{4}\left(\sum_{m=1}^{K}\mathsf{S}_{k,m}^t - \sum_{l=1}^{K}\mathsf{S}_{k,l}^t\right), \text{ using (36)}\\
&= 0,
\end{aligned}$$

which ends the proof.

Thanks to this property, it is now possible to give more insight in the structure of vector $\boldsymbol{C}$ (node P_q contribution to the diffusion flux). We introduce the matrix $\mathsf{D} = \mathsf{S}^t\mathsf{M}^{-1}\mathsf{S}$ which is a symmetric positive definite matrix. Hence, we have $\Gamma = -\frac{1}{4}(\mathsf{D} - \Lambda)$. As a corollary of property (45), D verifies the following property

$$\forall\ k = 1 \dots K \quad \sum_{l=1}^{K}\mathsf{D}_{k,l} = \alpha_k\lambda_k^2. \tag{46}$$

Moreover, since Λ is a diagonal matrix we get

$$\forall\ k \neq l \quad \Gamma_{k,l} = -\frac{1}{4}\mathsf{D}_{k,l}. \tag{47}$$

With the above results, one can transform the expression of C_k in the following way:

$$\begin{aligned} C_k &= \sum_{l=1}^{K} \Gamma_{k,l} u_l, \\ &= \sum_{l\neq k}^{K} \Gamma_{k,l} u_l + \Gamma_{k,k} u_k, \\ &= \sum_{l\neq k}^{K} \Gamma_{k,l} (u_l - u_k), \text{ using (45).} \end{aligned}$$

Finally, introducing D, one obtains

$$C_k = -\frac{1}{4} \sum_{l\neq k}^{K} \mathsf{D}_{k,l} (u_l - u_k). \tag{48}$$

This formula exhibits the fundamental role played by matrix $\mathsf{D} = \mathsf{S}^t \mathsf{M}^{-1} \mathsf{S}$. $\mathsf{D}_{k,l}$ has the physical dimension of a diffusion coefficient. It can be seen as the effective conductivity between the kth and the lth cells through vertex P_q. Thus, D is the effective conductivity tensor associated with node P_q.

3.3.2. Properties of matrices Γ and D

Before constructing the global diffusion matrix, we will give some useful properties for Γ and D.

First of all, we claim that Γ is a symmetric positive semi definite matrix

$$\forall\ \boldsymbol{U} = (u_1 \dots u_K)^t \quad (\Gamma \boldsymbol{U}, \boldsymbol{U}) \geqslant 0, \tag{49}$$

where (,) denotes the Euclidian dot product in $\mathbb{R}^K$. In order to show this fundamental result, we begin by expressing $(\Gamma \boldsymbol{U}, \boldsymbol{U})$ in terms of u_k and C_k. We notice that $(\Gamma \boldsymbol{U})_k = C_k$, hence

$$(\Gamma \boldsymbol{U}, \boldsymbol{U}) = \sum_{k=1}^{K} u_k C_k. \tag{50}$$

The proof is based on an integral interpretation of $(\Gamma \boldsymbol{U}, \boldsymbol{U})$. We consider the corner sub-cell Ω_k^q related to node P_q and cell Ω_k, see Fig. 7. This sub-cell is the quadrangle whose vertices are P_q, the midpoints of the edges k, $k+1$ and the centroid G_k of the cell Ω_k. We denote by Ω^q the domain around node P_q, defined by

$$\Omega^q = \bigcup_{q=1}^{K} \Omega_k^q. \tag{51}$$

The boundary of Ω^q is denoted by $\partial\Omega^q$ and it is displayed by a dashed line in Fig. 7. We recall that the approximation space for the scalar variable u is made of piecewise constant functions i.e., u_k denotes the constant value of u in the cell Ω_k. Thus, we get $\boldsymbol{\Phi} \cdot \boldsymbol{N} = 0$ on the dashed line and one can write

$$C_k = \frac{1}{2}(L_k \Phi_k^k + L_{k+1} \Phi_{k+1}^k), = \int_{\Omega_k^q} \nabla \cdot \boldsymbol{\Phi} \, \mathrm{d}\Omega,$$

where $\boldsymbol{\Phi} = -D \nabla \boldsymbol{u}$ is the diffusion flux. Therefore, one gets

$$u_k C_k = \int_{\Omega_k^q} u \nabla \cdot \boldsymbol{\Phi} \, \mathrm{d}\Omega. \tag{52}$$

Summing this formula over all sub-cells around node P_q gives us the integral representation

$$(\Gamma \boldsymbol{U}, \boldsymbol{U}) = \int_{\Omega^q} u \nabla \cdot \boldsymbol{\Phi} \, \mathrm{d}\Omega. \tag{53}$$

An integration by parts of the right-hand side yields

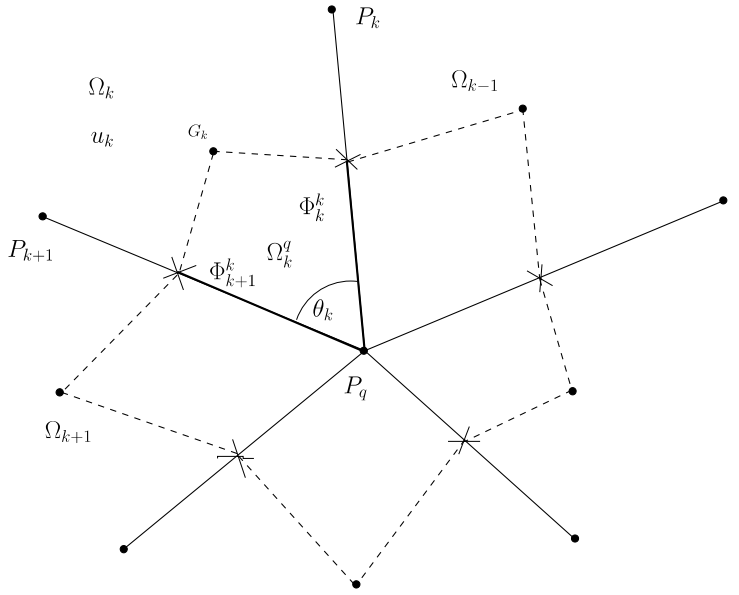

Fig. 7. Sub-cells around a node P_q.

$$\int_{\Omega^q} u\nabla\cdot\boldsymbol{\Phi}\,\mathrm{d}\Omega = \int_{\Omega^q}\nabla\cdot(u\boldsymbol{\Phi})\,\mathrm{d}\Omega - \int_{\Omega^q}\boldsymbol{\nabla}u\cdot\boldsymbol{\Phi}\,\mathrm{d}\Omega, = \int_{\partial\Omega^q} u\boldsymbol{\Phi}\cdot\boldsymbol{N}\,\mathrm{d}l + \int_{\Omega^q} D^{-1}\boldsymbol{\Phi}\cdot\boldsymbol{\Phi}\,\mathrm{d}\Omega.$$

Since $\boldsymbol{\Phi}\cdot\boldsymbol{N}=0$ on the dashed line, the boundary integral on the right-hand side is zero and one obtains the final result

$$(\Gamma\boldsymbol{U},\boldsymbol{U}) = \int_{\Omega^q} D^{-1}\boldsymbol{\Phi}\cdot\boldsymbol{\Phi}\,\mathrm{d}\Omega. \tag{54}$$

The right-hand side is always positive. This ends the proof.

Knowing that Γ is symmetric positive semi definite, it is clear that $\Gamma_{k,k}\geqslant 0$ for any $k=1\ldots K$. Since

$$\Gamma_{k,k} = -\sum_{l\neq k}^{K}\Gamma_{k,l}, = \frac{1}{4}\sum_{l\neq k}^{K}\mathsf{D}_{k,l},$$

we get the following property concerning D

$$\forall\ k=1\ldots K \quad \sum_{l\neq k}^{K}\mathsf{D}_{k,l}\geqslant 0. \tag{55}$$

3.3.3. The global diffusion matrix

Now, we collect the diffusion contributions for each internal node P_q and we build the global diffusion matrix denoted by A. We use the global numbering of cells, we recall that the local index k corresponds to the global index i, and we denote by j the global index corresponding to the local one l. The global diffusion matrix A is a $I\times I$ matrix which is defined by the following algorithm:

for $q\leftarrow 1\ldots Q_i$ **do**
  for $k\leftarrow 1\ldots K(q)$ **do**
  compute L_k, θ_k and $\alpha_k=\frac{D_k}{\omega_k}$
  endfor
  compute the $K\times K$ matrices M, S, M^{-1} and $\mathsf{D}=\mathsf{S}^t\mathsf{M}^{-1}\mathsf{S}$

```
for k ← 1 ... K(q) do
define i = i(k)
  for l ← 1 ... K(q) do
  define j = j(l)
    if i ≠ j then
    A_{i,i} = A_{i,i} + (1/4) D_{k,l}
    A_{i,j} = −(1/4) D_{k,l}
    endif
  endfor
endfor
endfor
```

We claim that A is a symmetric positive semi definite matrix, without taking account of the boundary conditions. This result lies in the fact that Γ is a symmetric positive semi definite matrix, since we have

$$[\mathsf{A}\mathscr{U}, \mathscr{U}] = \sum_{q=1}^{Q_i} (\Gamma^q \boldsymbol{U}, \boldsymbol{U}), \tag{56}$$

where $\mathscr{U} = (u_1 \dots u_I)^t$ is the global vector of mean values, [,] denotes the Euclidian dot product in $\mathbb{R}^I$ and Γ^q is the Γ matrix attached to node P_q.

Comment 3. In order to evaluate numerically matrix D, we need to compute the inverse of M. This computation is done for each node P_q. It is based on the Cholesky decomposition of M, since M is symmetric definite positive.

Finally, we can build the stencil associated with our diffusion scheme. The cells k and l exchange diffusion flux through node P_q by the mean of $\Gamma_{k,l}$. Hence, the stencil corresponding to a global cell Ω_i is built with all the neighbor cells of Ω_i which share a common node with the target cell. The stencil of our new diffusion scheme is local, see Fig. 8. Moreover, one obtains a nine-point scheme for a structured quadrilateral mesh.

Comment 4. We claim that A is an M-matrix if the following geometric conditions are fulfilled

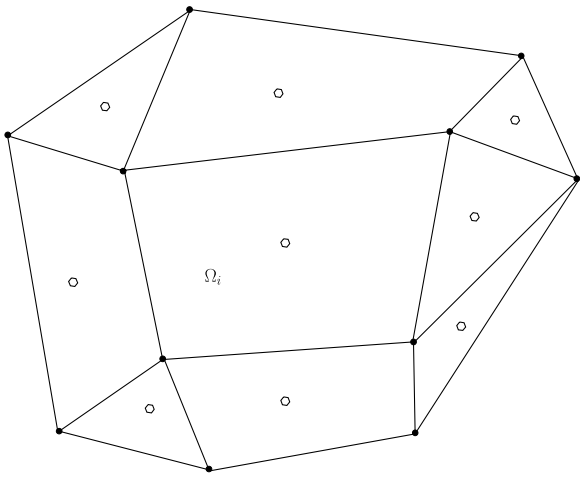

Fig. 8. Stencil for the diffusion scheme.

$$\theta_k \in \left[-\frac{\pi}{2},\frac{\pi}{2}\right], \quad \forall\, k = 1 \ldots K,$$
$$\cos\theta_k \leqslant \min\left(\frac{L_k}{L_{k+1}},\frac{L_{k+1}}{L_k}\right). \tag{57}$$

Note that these conditions have been already presented, see Comment 2. We recall that the first condition implies that M is an M-matrix, and the second $\mathsf{S}_{k,l} \geqslant 0$. Thus $\mathsf{D} = \mathsf{S}^t\mathsf{M}^{-1}\mathsf{S}$ is such that $\mathsf{D}_{k,l} \geqslant 0$. Consequently, A is a symmetric positive semi definite matrix whose coefficients verify $\mathsf{A}_{i,i} \geqslant 0$ and $\mathsf{A}_{i,j} \leqslant 0$. Note that the geometric conditions (35) are very restrictive and could be violated with distorted grids. However it will be a useful criterion in order to detect the occurrence of maximum principle violation.

3.4. Boundary conditions

In this section we deal with the discretization of boundary conditions on $\partial\Omega$. We will consider a boundary vertex, i.e. $P_q \in \partial\Omega$, for $q = Q_i + 1 \ldots Q_i + Q_e$ where Q_e denotes the number of boundary nodes. We shall show how to build its contribution to the diffusion matrix A. The boundary conditions are imposed on the boundary edges which are connected to P_q. These conditions will be of two types: Neumann (imposed flux) or Dirichlet (imposed value of u).

3.4.1. Neumann boundary conditions

Let P_q be a boundary node. We define as usual a local numbering for the cells and the edges which are connected to P_q, see Fig. 9. The number of cells is denoted by $K = K(q)$, therefore there are $K+1$ edges. The first and last edges are located on the boundary. Normal fluxes imposed on these two edges are denoted by $\Phi_1^\star$ and $\Phi_{K+1}^\star$. Notice that if $\Phi_1^\star > 0$, then we have an outward flux and if $\Phi_1^\star < 0$, we have an inward flux. As for internal nodes, the first step is to express the face values in terms of the mean values, using the continuity of the normal flux across the edges. We define the face values vector $\bar{\boldsymbol{U}} = (\bar{u}_1 \ldots \bar{u}_{K+1})^t$ and the mean values vector $\boldsymbol{U} = (u_1 \ \ldots u_K)^t$. Let us notice that $\bar{\boldsymbol{U}} \in \mathbb{R}^{K+1}$ and $\boldsymbol{U} \in \mathbb{R}^K$ since we have K cells and $K+1$ edges. There are $K+1$ unknown face values, hence we need $K+1$ equations. These equations are given by the continuity of normal fluxes across the $K+1$ edges. We denote by Φ_k^k the normal flux on the kth edge seen from the kth cell and by Φ_k^{k-1} the normal flux on the kth edge seen from the $(k-1)$th cell, for $k = 2 \ldots K$. The continuity conditions are

- First edge $k = 1$

$$L_1\Phi_1^1 = L_1\Phi_1^\star.$$

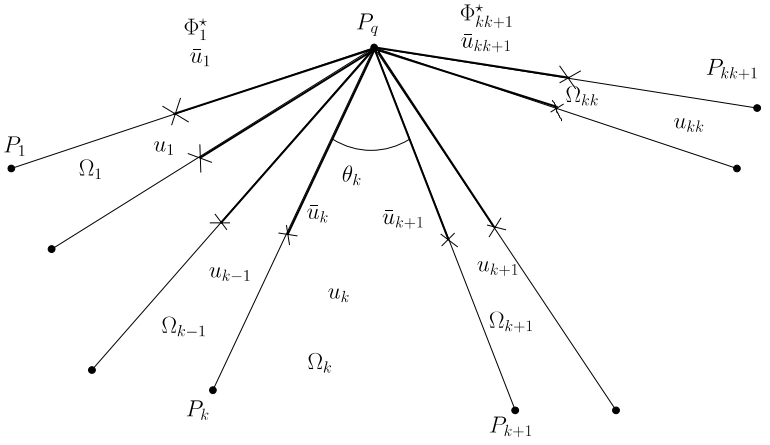

Fig. 9. Local numbering around a boundary node P_q.

- Internal edges $k = 2 \dots K$

  $L_k(\Phi_k^{k-1} + \Phi_k^k) = 0.$

- Last edge $k = K + 1$

  $L_{K+1}\Phi_{K+1}^K = L_{K+1}\Phi_{K+1}^\star.$

Once we have expressed the fluxes Φ_k^k in terms of $\bar{u}_k$ and u_k, these $K+1$ continuity conditions provide $K+1$ equations for the $K+1$ unknowns $\bar{u}_k$. We recall the expressions of Φ_k^k and Φ_k^{k-1}

$$\Phi_k^{k-1} = -\frac{1}{2}\alpha_{k-1}[-\cos\theta_{k-1}L_{k-1}(\bar{u}_{k-1} - u_{k-1}) + L_k(\bar{u}_k - u_{k-1})],$$
$$\Phi_k^k = -\frac{1}{2}\alpha_k[L_k(\bar{u}_k - u_k) - \cos\theta_k L_{k+1}(\bar{u}_{k+1} - u_k)],$$

where $\alpha_k = \frac{D_k}{\omega_k}$ is assumed to be a real and non negative number. After substituting the flux expressions into the continuity conditions, one obtains the following linear system with $K+1$ equations

- First row

$$\alpha_1 L_1^2\bar{u}_1 - \alpha_1\cos\theta_1 L_1 L_2\bar{u}_2 = \alpha_1 L_1(L_1 - L_2\cos\theta_1)u_1 - 2L_1\Phi_1^\star, \tag{58}$$

- kth row, $k = 2 \dots K$

$$\begin{aligned}&-\alpha_{k-1}\cos\theta_{k-1}L_{k-1}L_k\bar{u}_{k-1} + (\alpha_{k-1} + \alpha_k)L_k^2\bar{u}_k - \alpha_k\cos\theta_k L_k L_{k+1}\bar{u}_{k+1}\\ &\quad = \alpha_{k-1}L_k(L_k - L_{k-1}\cos\theta_{k-1})u_{k-1} + \alpha_k L_k(L_k - L_{k+1}\cos\theta_{k+1})u_k,\end{aligned} \tag{59}$$

- last row

$$-\alpha_K\cos\theta_K L_K L_{K+1}\bar{u}_K + \alpha_K L_{K+1}^2\bar{u}_{K+1} = \alpha_K L_{K+1}(L_{K+1} - L_K\cos\theta_K)u_K - 2L_{K+1}\Phi_{K+1}^\star. \tag{60}$$

Let us notice that this system is similar to the one obtained at the internal node. The main difference lies in the fact that we do not have an equal number of cells and edges. Therefore, the first and last rows are different. As in Section 3.1.2, we put this system into a matrix form. The matrix associated to the linear system is denoted by $\widetilde{\mathsf{M}}$. It is a $(K+1)\times(K+1)$ tridiagonal matrix. The non zero terms are

- First row:

  $\widetilde{\mathsf{M}}_{1,1} = \alpha_1 L_1^2,$

  $\widetilde{\mathsf{M}}_{1,2} = -\alpha_1\cos\theta_1 L_1 L_2,$

- kth row $k = 2 \dots K$:

  $\widetilde{\mathsf{M}}_{k,k-1} = -\alpha_{k-1}\cos\theta_{k-1}L_{k-1}L_k,$

  $\widetilde{\mathsf{M}}_{k,k} = (\alpha_{k-1} + \alpha_k)L_k^2,$

  $\widetilde{\mathsf{M}}_{k,k+1} = -\alpha_k\cos\theta_k L_k L_{k+1},$

- Last row:

  $\widetilde{\mathsf{M}}_{K,K+1} = -\alpha_K\cos\theta_K L_K L_{K+1},$

  $\widetilde{\mathsf{M}}_{K+1,K+1} = \alpha_K L_{K+1}^2.$

It is clear that $\widetilde{\mathsf{M}}$ is a symmetric matrix. Using the same decomposition as in Section 3.1.2, we show that $\widetilde{\mathsf{M}}$ is positive definite. Finally, $\widetilde{\mathsf{M}}$ is symmetric positive definite and the linear system for the face values $\bar{u}_k$ has always a unique solution.

The right-hand sides of (58)–(60) are rewritten in a more concise form by introducing the sparse matrix $\widetilde{\mathsf{S}}$. This matrix has $K+1$ rows and K columns since $\bar{\boldsymbol{U}} \in \mathbb{R}^{K+1}$ and $\boldsymbol{U} \in \mathbb{R}^{K}$. Its non zero terms are defined by

$$\begin{aligned}
&\widetilde{\mathsf{S}}_{1,1} = \alpha_1 L_1 (L_1 - L_2 \cos\theta_1),\\
&\forall\ k = 2 \ldots K \quad \widetilde{\mathsf{S}}_{k,k-1} = \alpha_{k-1} L_k (L_k - L_{k-1} \cos\theta_{k-1}),\\
&\forall\ k = 2 \ldots K \quad \widetilde{\mathsf{S}}_{k,k} = \alpha_k L_k (L_k - L_{k+1} \cos\theta_k),\\
&\widetilde{\mathsf{S}}_{K+1,K} = \alpha_K L_{K+1} (L_{K+1} - L_K \cos\theta_K).
\end{aligned}$$

Finally, we introduce the vector $\boldsymbol{B} \in \mathbb{R}^{K+1}$ which takes into account the boundary conditions

$$\begin{aligned}
&B_1 = 2 L_1 \Phi_1^{\star},\\
&\forall\ k = 2 \ldots K \quad B_k = 0,\\
&B_{K+1} = 2 L_{K+1} \Phi_{K+1}^{\star}.
\end{aligned}$$

With all these notations, the linear system (58)–(60) reduces to

$$\widetilde{\mathsf{M}}\,\bar{\boldsymbol{U}} = \widetilde{\mathsf{S}}\,\boldsymbol{U} - \boldsymbol{B}. \tag{61}$$

As in Section 3.1.2, we introduce $\widetilde{\mathsf{F}} = \widetilde{\mathsf{M}}^{-1}\widetilde{\mathsf{S}}$. This rectangular matrix has $K+1$ rows and K columns and verifies the following property:

$$\forall\ k = 1 \ldots K+1 \sum_{l=1}^{K} \widetilde{\mathsf{F}}_{k,l} = 1. \tag{62}$$

This property is similar to property (36) satisfied by F . Its demonstration is based on the same argument, i.e.

$$\forall\ k = 1 \ldots K \sum_{l=1}^{K+1} \widetilde{\mathsf{M}}_{k,l} = \sum_{l=1}^{K} \widetilde{\mathsf{S}}_{k,l}.$$

Hence, if $\boldsymbol{U}$ is a uniform vector field and $\boldsymbol{B} = \boldsymbol{0}$, then $\bar{\boldsymbol{U}}$ is also uniform with the same constant value.

In order to achieve the construction of the diffusion matrix, we are going to evaluate the contribution of the node P_q to the diffusion flux, as we have done in Section 3.3. We use the same notations. This node contribution for cell $k = k(i)$ is expressed by

$$\widetilde{C}_k = \frac{1}{2}(L_k \Phi_k^k + L_{k+1} \Phi_{k+1}^k).$$

In order to compute $\widetilde{C}_k$, we substitute the expressions of Φ_k^k and Φ_{k+1}^k coming from (40). Then, one obtains

$$\begin{aligned}
\widetilde{C}_k &= -\frac{\alpha_k}{4}[L_k(L_k - L_{k+1}\cos\theta_k)(\bar{u}_k - u_k) + L_{k+1}(L_{k+1} - L_k \cos\theta_k)(\bar{u}_{k+1} - u_k)],\\
\widetilde{C}_k &= -\frac{1}{4}[\widetilde{\mathsf{S}}_{k,k}(\bar{u}_k - u_k) + \widetilde{\mathsf{S}}_{k+1,k}(\bar{u}_{k+1} - u_k)],\\
\widetilde{C}_k &= -\frac{1}{4}\left[\sum_{l=1}^{K+1} \widetilde{\mathsf{S}}_{l,k}(\bar{u}_l - u_l)\right],\\
\widetilde{C}_k &= -\frac{1}{4}\left[\sum_{l=1}^{K+1} \widetilde{\mathsf{S}}^t_{k,l}(\bar{u}_l - u_l)\right].
\end{aligned}$$

Here $\widetilde{\mathsf{S}}^t$ is the transpose of S. We notice that $\widetilde{\mathsf{S}}^t$ is a rectangular matrix with K rows and $K+1$ columns. As in Section 3.3, we can write

$$\forall\ k = 1 \ldots K \quad \sum_{l=1}^{K+1} \widetilde{\mathsf{S}}^t_{k,l} = \widetilde{\mathsf{S}}_{k,k} + \widetilde{\mathsf{S}}_{k+1,k}, = \alpha_k (L_k^2 + L_{k+1}^2 - 2 L_k L_{k+1} \cos\theta_k) > 0,$$

since $\alpha_k > 0$. As previously, we introduce the length λ_k

$$\lambda_k^2 = L_k^2 + L_{k+1}^2 - 2L_kL_{k+1}\cos\theta_k,$$

and the diagonal $K\times K$ matrix Λ defined by

$$\Lambda_{k,l} = \alpha_k\lambda_k^2\delta_{k,l}.$$

Recalling that $\bar{U} = \widetilde{\mathsf{M}}^{-1}\widetilde{\mathsf{S}}\boldsymbol{U} - \widetilde{\mathsf{M}}^{-1}\boldsymbol{B}$ we obtain for the vector $\widetilde{\boldsymbol{C}} = (\widetilde{C}_1 \dots \widetilde{C}_K)^t$ the final expression

$$\widetilde{\boldsymbol{C}} = -\frac{1}{4}\left(\widetilde{\mathsf{S}}^t\widetilde{\mathsf{M}}^{-1}\widetilde{\mathsf{S}} - \Lambda\right)\boldsymbol{U} + \frac{1}{4}\widetilde{\mathsf{S}}^t\widetilde{\mathsf{M}}^{-1}\boldsymbol{B}. \tag{63}$$

It is useful to introduce the $K\times K$ matrix $\widetilde{\Gamma}$ defined by

$$\widetilde{\Gamma} = -\frac{1}{4}(\widetilde{\mathsf{S}}^t\widetilde{\mathsf{M}}^{-1}\widetilde{\mathsf{S}} - \Lambda). \tag{64}$$

$\widetilde{\Gamma}$ is symmetric positive semi definite. The proof is similar to the one we have presented in Section 3.3.2. Moreover, it satisfies the conservativity property

$$\forall\ k = 1\dots K \quad \sum_{l=1}^{K}\widetilde{\Gamma}_{k,l} = 0. \tag{65}$$

The reasoning to obtain the above result used property (62). The demonstration is the same as in Section 3.3. Therefore if $\boldsymbol{U}$ is a uniform vector field and $\boldsymbol{B} = \boldsymbol{0}$ then $\widetilde{\Gamma}\boldsymbol{U} = \boldsymbol{0}$ and $\widetilde{\boldsymbol{C}} = \boldsymbol{0}$. Then, the diffusion fluxes around P_q are zero. Using 65 we can rewrite $\widetilde{\boldsymbol{C}}$ in the following way:

$$\widetilde{C}_k = \sum_{l=1}^{K}\widetilde{\Gamma}_{k,l}u_l + \frac{1}{4}(\widetilde{\mathsf{S}}^t\widetilde{\mathsf{M}}^{-1}\boldsymbol{B})_k, = \sum_{l\neq k}^{K}\widetilde{\Gamma}_{k,l}u_l + \widetilde{\Gamma}_{k,k}u_k + \frac{1}{4}(\widetilde{\mathsf{S}}^t\widetilde{\mathsf{M}}^{-1}\boldsymbol{B})_k, = \sum_{l\neq k}^{K}\widetilde{\Gamma}_{k,l}(u_l - u_k) + \frac{1}{4}(\widetilde{\mathsf{S}}^t\widetilde{\mathsf{M}}^{-1}\boldsymbol{B})_k.$$

Finally, we introduce $\widetilde{\mathsf{D}} = \widetilde{\mathsf{S}}^t\widetilde{\mathsf{M}}^{-1}\widetilde{\mathsf{S}}$. We remark that $\widetilde{\mathsf{D}}$ is a $K\times K$ symmetric positive definite matrix. Then $\widetilde{C}_k$ is given by

$$\widetilde{C}_k = -\frac{1}{4}\sum_{l\neq k}^{K}\widetilde{\mathsf{D}}_{k,l}(u_l - u_k) + \frac{1}{4}(\widetilde{\mathsf{S}}^t\widetilde{\mathsf{M}}^{-1}\boldsymbol{B})_k. \tag{66}$$

This final expression of $\widetilde{C}_k$ is very close to the expression we have obtained for C_k in Section 3.3. The matrix $\widetilde{\mathsf{D}}$ is the effective conductivity between the kth and the lth cell through node P_q. Moreover, the Neumann boundary conditions are expressed by the term $\frac{1}{4}(\widetilde{\mathsf{S}}^t\widetilde{\mathsf{M}}^{-1}\boldsymbol{B})_k$. Finally, we collect the contribution of each boundary vertex P_q in order to finish the construction of the global diffusion matrix. We give the following algorithm

for $q \leftarrow Q_i + 1 \dots Q_i + Q_e$ **do**
  for $k \leftarrow 1 \dots K(q)$ **do**
  compute θ_k and $\alpha_k = \frac{D_k}{\omega_k}$
  endfor
  compute the matrices $\widetilde{\mathsf{M}}$, $\widetilde{\mathsf{S}}$,
  $\widetilde{\mathsf{M}}^{-1}$ and $\widetilde{\mathsf{D}} = \widetilde{\mathsf{S}}^t\widetilde{\mathsf{M}}^{-1}\widetilde{\mathsf{S}}$
  for $k \leftarrow 1 \dots K(q)$ **do**
  define $i = i(k)$
    for $l \leftarrow 1 \dots K(q)$ **do**
    define $j = j(l)$
      if $i \neq j$ **then**
      $\mathsf{A}_{i,i} = \mathsf{A}_{i,i} + \frac{1}{4}\mathsf{D}_{k,l}$
      $\mathsf{A}_{i,j} = -\frac{1}{4}\mathsf{D}_{k,l}$
      endif
    endfor
  endfor
endfor

Here, i denotes the global index of cell k, and j the global index of cell l. We have achieved the construction of the global diffusion matrix. It is a symmetric positive semi definite matrix, since $\widetilde{\Gamma}$ is also symmetric positive semi definite matrix. Using (45) and (65), it is clear that A is a $I \times I$ matrix which verifies

$$\forall\ i = 1 \dots I \quad \sum_{j=1}^{I} \mathsf{A}_{i,j} = 0. \tag{67}$$

This property implies the global conservativity for the diffusion scheme for homogeneous Neumann boundary conditions, i.e. $\boldsymbol{B} = \mathbf{0}$.

We denote by $\mathscr{R} = (\mathscr{R}_1 \dots \mathscr{R}_I)$ the right-hand side of the global diffusion system. Its ith component is given by

$$\mathscr{R}_i = -\frac{1}{4}(\widetilde{\mathsf{S}}^t \widetilde{\mathsf{M}}^{-1} \boldsymbol{B})_k. \tag{68}$$

3.4.2. Dirichlet boundary conditions

In this section we restrict ourselves to the simple cases $K = 1$ (corner vertex) and $K = 2$ because the calculations are explicit. However, the general case $K > 2$ presents no difficulties and it can be treated using the same methodology as the one presented in Section 3.4.1

The case $K = 1$

We consider here a corner vertex P_q which is located on the boundary $\partial\Omega$. The two edges which are connected by P_q are labeled 1 and 2. We denoted by $u_1^\star$ and $u_2^\star$ the face values imposed on these edges, see Fig. 10. Then we have $\bar{u}_1 = u_1^\star$ and $\bar{u}_2 = u_2^\star$. The face values are known, so we have just to compute the normal fluxes. The calculation is straightforward and we get

$$\Phi_1^1 = -\frac{\alpha_1}{2}[L_1(u_1^\star - u_1) - \cos\theta_1 L_2(u_2^\star - u_1)],$$
$$\Phi_2^1 = -\frac{\alpha_1}{2}[-\cos\theta_1 L_1(u_1^\star - u_1) + L_2(u_2^\star - u_1)].$$

From the fluxe expressions we deduce the node P_q contribution to the flux for cell Ω_1. This contribution is given by

$$C_1 = \frac{1}{2}(L_1\Phi_1^1 + L_2\Phi_2^1),$$
$$= \frac{\alpha_1}{4}\lambda_1^2 u_1 - \frac{\alpha_1}{4}L_1(L_1 - L_2\cos\theta_1)u_1^\star - \frac{\alpha_1}{4}L_2(L_2 - L_1\cos\theta_1)u_2^\star,$$

where $\lambda_1^2 = L_1^2 + L_2^2 - 2L_1L_2\cos\theta_1$.

If i denotes the global index of cell 1 in the global numbering, then C_1 contributes to the diffusion matrix A as follows:

$$\mathsf{A}_{i,i} = \frac{\alpha_1}{4}\lambda_1^2. \tag{69}$$

We remark that the C_1 contribution to the diagonal is non negative. Therefore A is a symmetric positive definite matrix. The contribution to the right-hand side $\mathscr{R}$ is given by

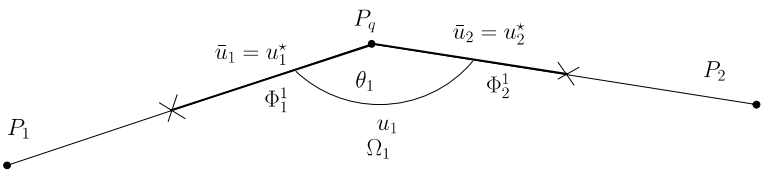

Fig. 10. Dirichlet, case $K = 1$, local numbering around boundary corner node P_q.

$$\mathscr{R}_i = \frac{\alpha_1}{4} L_1 (L_1 - L_2 \cos\theta_1) u_1^\star + \frac{\alpha_1}{4} L_2 (L_2 - L_1 \cos\theta_1) u_2^\star. \tag{70}$$

The case $K = 2$

In this subsection we consider a boundary node P_q which is not a corner. This is the general case for a quadrangular mesh. Since $K = 2$ this node connects three edges labeled 1, 2 and 3, see Fig. 11. Face values are imposed on edges 1 and 3 and they are denoted by $u_1^\star$ and $u_3^\star$. Hence, we have $\bar{u}_1 = u_1^\star$, $\bar{u}_3 = u_3^\star$ and we are going to compute $\bar{u}_2$ using normal flux continuity across edge 2. In order to do so, we recall the expressions of the normal fluxes

$$\begin{aligned}
\Phi_1^1 &= -\frac{\alpha_1}{2}[L_1(u_1^\star - u_1) - \cos\theta_1 L_2(\bar{u}_2 - u_1)],\\
\Phi_2^1 &= -\frac{\alpha_1}{2}[-\cos\theta_1 L_1(u_1^\star - u_1) + L_2(\bar{u}_2 - u_1)],\\
\Phi_2^2 &= -\frac{\alpha_2}{2}[L_2(\bar{u}_2 - u_2) - \cos\theta_2 L_3(u_3^\star - u_2)],\\
\Phi_3^2 &= -\frac{\alpha_2}{2}[-\cos\theta_2 L_2(\bar{u}_2 - u_2) + L_3(u_3^\star - u_2)].
\end{aligned}$$

The continuity of normal flux on edge 2 is given by

$$\frac{1}{2}(L_2\Phi_2^1 + L_2\Phi_2^2) = 0.$$

It enables us to obtain the face value on edge 2 in terms of the mean values u_1 and u_2:

$$\bar{u}_2 = \frac{\alpha_1 u_1 + \alpha_2 u_2}{\alpha_1 + \alpha_2} + \frac{\alpha_1 \cos\theta_1 L_1}{(\alpha_1 + \alpha_2)L_2}(u_1^\star - u_1) + \frac{\alpha_2 \cos\theta_2 L_3}{(\alpha_1 + \alpha_2)L_2}(u_3^\star - u_2). \tag{71}$$

If $\theta_1 = \theta_2 = \frac{\pi}{2}$ (rectangular cells), then we recover the classical interpolation obtained with a five-point scheme.

In order to achieve the building of the diffusion matrix A, we compute the node P_q contribution to the flux as we have done previously. We compute C_1 and C_2 knowing that

$$\begin{aligned}
C_1 &= \frac{1}{2}(L_1\Phi_1^1 + L_2\Phi_2^1),\\
C_2 &= \frac{1}{2}(L_2\Phi_2^2 + L_3\Phi_3^2).
\end{aligned}$$

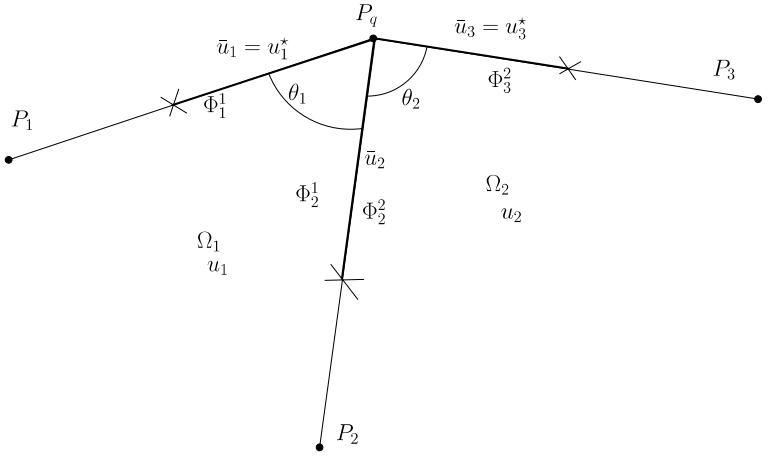

Fig. 11. Dirichlet, case $K = 2$, local numbering around boundary node P_q.

Finally, after substituting the expression of $\bar{u}_2$ in the normal fluxes, one obtains the following results:

$$C_1 = \gamma_{1,1}u_1 + \gamma_{1,2}u_2 + \sigma_1,$$
$$C_2 = \gamma_{2,1}u_1 + \gamma_{2,2}u_2 + \sigma_2,$$

where the coefficients of the 2×2 matrix γ are given by

$$\gamma_{1,1} = \frac{\alpha_1}{4(\alpha_1+\alpha_2)}(\alpha_1 \sin^2\theta_1 L_1^2 + \alpha_2\lambda_1^2),$$
$$\gamma_{1,2} = -\frac{\alpha_1\alpha_2}{4(\alpha_1+\alpha_2)}[(L_2 - L_1\cos\theta_1)(L_2 - L_3\cos\theta_2)],$$
$$\gamma_{2,1} = -\frac{\alpha_1\alpha_2}{4(\alpha_1+\alpha_2)}[(L_2 - L_1\cos\theta_1)(L_2 - L_3\cos\theta_2)],$$
$$\gamma_{2,2} = \frac{\alpha_2}{4(\alpha_1+\alpha_2)}(\alpha_2 \sin^2\theta_2 L_3^2 + \alpha_1\lambda_2^2).$$

We recall that $\lambda_1^2 = L_1^2 + L_2^2 - 2L_1L_2\cos\theta_1$ and $\lambda_2^2 = L_2^2 + L_3^2 - 2L_2L_3\cos\theta_2$, hence $\gamma_{1,1}$ and $\gamma_{2,2}$ are non negative. Moreover γ is symmetric. The boundary conditions contribution is given by

$$\sigma_1 = -\frac{\alpha_1}{4(\alpha_1+\alpha_2)}[L_1\{\alpha_1\sin^2\theta_1 L_1 + \alpha_2(L_1 - L_2\cos\theta_1)\}u_1^\star + \alpha_2\cos\theta_2 L_3(L_2 - L_1\cos\theta_1)u_3^\star],$$
$$\sigma_2 = -\frac{\alpha_2}{4(\alpha_1+\alpha_2)}[\alpha_1\cos\theta_1 L_1(L_2 - L_3\cos\theta_2)u_1^\star + L_3\{\alpha_2\sin^2\theta_2 L_3 + \alpha_1(L_3 - L_2\cos\theta_2)\}u_3^\star].$$

If i denotes the global index of cell 1 and j the global index of cell *2* in the global numbering, then C_1 and C_2 contribute to the diffusion matrix A as follows:

$$\begin{aligned} \mathsf{A}_{i,i} &= \gamma_{1,1},\\ \mathsf{A}_{i,j} &= \gamma_{1,2},\\ \mathsf{A}_{j,i} &= \gamma_{2,1},\\ \mathsf{A}_{j,j} &= \gamma_{2,2}. \end{aligned} \tag{72}$$

Note that $\gamma_{1,1} > 0$ and $\gamma_{1,1}\gamma_{2,2} - \gamma_{1,2}^2 > 0$, hence the following matrix:

$$\begin{pmatrix} \gamma_{1,1} & \gamma_{1,2} \\ \gamma_{1,2} & \gamma_{2,2} \end{pmatrix},$$

is symmetric positive definite. Therefore, A is also a symmetric positive definite matrix. The contribution to the right-hand side $\mathscr{R}$ is given by

$$\begin{aligned} \mathscr{R}_i &= -\sigma_1,\\ \mathscr{R}_j &= -\sigma_2. \end{aligned} \tag{73}$$

4. Time discretization

In this section we will briefly describe the time discretization of our diffusion problem. For the sake of simplicity, we make the assumption that ρ and C are independent of u.

First of all, we recall some notations. We denote by $\mathscr{U} = (u_1 \dots u_I)^t$ the vector of cell centered unknowns, where I is the total number of cells. After spatial discretization we have obtained the global diffusion matrix A which includes the boundary conditions. A is a $I\times I$ symmetric matrix which is at least positive semi definite. We have introduced the right-hand side corresponding to boundary conditions: $\mathbf{R} = (\mathscr{R}_1 \dots \mathscr{R}_I)^t$. With these notations, $\mathscr{U}$ is the solution of the following system of differential equations:

$$\mathsf{M}C\frac{\mathrm{d}\mathscr{U}}{\mathrm{d}t} + \mathsf{A}\mathscr{U} = \mathscr{R}. \tag{74}$$

MC is the diagonal matrix defined by $(\mathrm{MC})_{i,i} = m_i C_i$, where m_i and C_i are respectively the mass and the calorific capacity of the cell Ω_i.

We solve (74) on the time interval $[0,T]$. Let $0 = t^1 < t^2 < \cdots < t^n < t^{n+1} < \cdots < t^N = T$ be a subdivision of this interval. We denote the generic time step by $\Delta t = t^{n+1} - t^n$. In order to avoid a too small time step we will use a fully implicit discretization. After integration of (74) over $[t^n, t^{n+1}]$ one obtains

$$\mathrm{MC}(\mathscr{U}^{n+1} - \mathscr{U}^n) + \Delta t \mathsf{A}^n \mathscr{U}^{n+1} = \Delta t \mathscr{R}^n. \tag{75}$$

For non linear heat conduction problems the diffusion coefficient is a function of the temperature, namely $D \equiv D(u)$. In this case, the diffusion coefficient is evaluated at the beginning of the time step and we set $D^n = D(u^n)$. By this way, one computes the global matrix diffusion at time t^n and denotes it by A^n. Thus, $\mathscr{U}^{n+1}$ is the solution of the linear system:

$$(\mathrm{MC} + \Delta t \mathsf{A}^n)\mathscr{U}^{n+1} = \mathrm{MC}\mathscr{U}^n + \Delta t \mathscr{R}^n. \tag{76}$$

Since A^n is at least symmetric positive semi definite and MC is such that $(\mathrm{MC})_{i,i} > 0$ then $\mathrm{MC} + \Delta t \mathsf{A}^n$ is symmetric positive definite. Consequently, this system admits always a unique solution.

Since $\mathrm{MC} + \Delta t \mathsf{A}^n$ is symmetric positive definite, the linear system (76) is solved by a classical conjugate gradient method coupled with an incomplete Cholesky preconditioner, see [13].

5. Numerical tests

We present the results obtained with our new scheme for several test cases. First, we focus on results obtained with triangular meshes. For these grids we show that our scheme preserves linear solutions. We also perform a standard convergence analysis for a non linear test case. This study provides a second order convergence rate.

Then, we present the results obtained for quadrangular grids. When the quadrangular cells are parallelograms, we show that the linear solutions are preserved. We proceed by studying the convergence rate for distorted quadrangular grids. For smooth grids, we get almost second order accuracy whereas the results obtained for random grids suggest that the scheme does not converge on such meshes. We also demonstrate numerically that our scheme is more accurate than the Kershaw scheme by performing a convergence analysis on an analytical test case.

All the tests presented here are classical and some of them can be found in [25,18,17]. Moreover, these tests have always an analytical solution, except the last one. We briefly describe the methodology used in order to perform the convergence analysis. For each calculation, the mesh resolution is characterized by the parameter

$$h = \sqrt{\frac{V_\Omega}{I}},$$

where V_Ω is the entire domain volume and I is the number of cell (triangular or quadrangular). We consider a grid whose mesh resolution is h and we denote by $\hat{u}_i^h$ the value of the analytical solution computed at the centroïd of the cell Ω_i. Let u_i^h be the numerical solution in the same cell. Then, we define for this mesh the asymptotic errors using both the maximum norm and the mean-square norm

$$\begin{aligned} E_{\max}^h &= \max_{i=1\ldots I} |u_i^h - \hat{u}_i^h|, \\ E_{\mathrm{l}_2}^h &= \sqrt{\sum_{i=1}^{I} (u_i^h - \hat{u}_i^h)^2 V_i}. \end{aligned} \tag{77}$$

The asymptotic error for both norms is estimated by

$$E^h = Ch^q + \mathrm{O}(h^{q+1}),$$

where q is the order of truncation error and C the convergence rate-constant which is independent of h. In the numerical examples, the asymptotic errors are evaluated on a sequence of grids with three different values of h.

Typically, for quadrangular grids we use h, $h/2$ and $h/4$. For two grids characterized by the mesh parameters h_1 and h_2 the order of convergence is evaluated using

$$q = \frac{\log\left(\frac{E^{h_1}}{E^{h_2}}\right)}{\log\left(\frac{h_1}{h_2}\right)}. \tag{78}$$

Almost all test cases are performed on a standard test problem which consists in solving the following diffusion equation in the unit square $0 \leqslant x, y \leqslant 1$

$$\begin{aligned} &\rho C \frac{\partial u}{\partial t} - \nabla \cdot (D \mathbf{\nabla} u) = S, \quad (x,y) \in \Omega, \\ &u(x,y,0) = u^0(x,y), \end{aligned} \tag{79}$$

where $S = S(x,y)$ is a source term. The standard initial condition is $u^0(x,y) = 0$. The values for the density and the calorific capacity are $\rho = 1$ and $C = 1$. We notice that almost all the analytical solutions are stationary. Therefore, we run our simulations until a steady state is reached. The boundary conditions, the source term and the scalar conductivity will be prescribed for each test case.

Finally, we present an unsteady non linear heat conduction problem. The aim of this test is to show the accuracy of our scheme on a polar distorted grid in comparison with the classical five-point scheme and with the Kershaw scheme.

5.1. Triangular mesh

5.1.1. A discontinuous conductivity problem

For this test the boundary conditions are defined by

$$\begin{aligned} &D\frac{\partial u}{\partial y} = 0 \text{ at } y = 0, \quad D\frac{\partial u}{\partial y} = 0 \text{ at } y = 1, \\ &u = 0 \text{ at } y = 0, \quad u = 1 \text{ at } y = 1. \end{aligned} \tag{80}$$

The conductivity $D = D(x,y)$ is discontinuous and given by

$$\begin{aligned} &0 \leqslant x \leqslant \frac{1}{2} \quad D = D_1, \\ &\frac{1}{2} \leqslant x \leqslant 1 \quad D = D_2. \end{aligned} \tag{81}$$

We set $S = 0$ and the stationary solution is

$$\begin{aligned} &0 \leqslant x \leqslant \frac{1}{2} \quad u(x,y) = 2\frac{D_2}{D_1 + D_2}x, \\ &\frac{1}{2} \leqslant x \leqslant 1 \quad u(x,y) = \frac{D_2 - D_1}{D_1 + D_2} + 2\frac{D_1}{D_1 + D_2}x. \end{aligned} \tag{82}$$

For the numerical application we use $D_1 = 1$ and $D_2 = 10$. We perform the calculation on an unstructured triangular mesh which is displayed in Fig. 12(left). This mesh is composed of 246 triangular cells. The isolines of the numerical steady-state solution are shown in Fig. 12(right). They are vertical straight lines. In addition, the asymptotic errors obtained are equal to zero up to machine precision. Thus, our scheme reproduces exactly the linear solution.

5.1.2. Discontinuous tangential flux

This particular problem is taken from [25] and can also be found in [26]. It has been designed in order to exhibit a discontinuous tangential flux at an interface. Thus, the goal of this case is to test the ability of our scheme to correctly reproduce this discontinuous tangential flux.

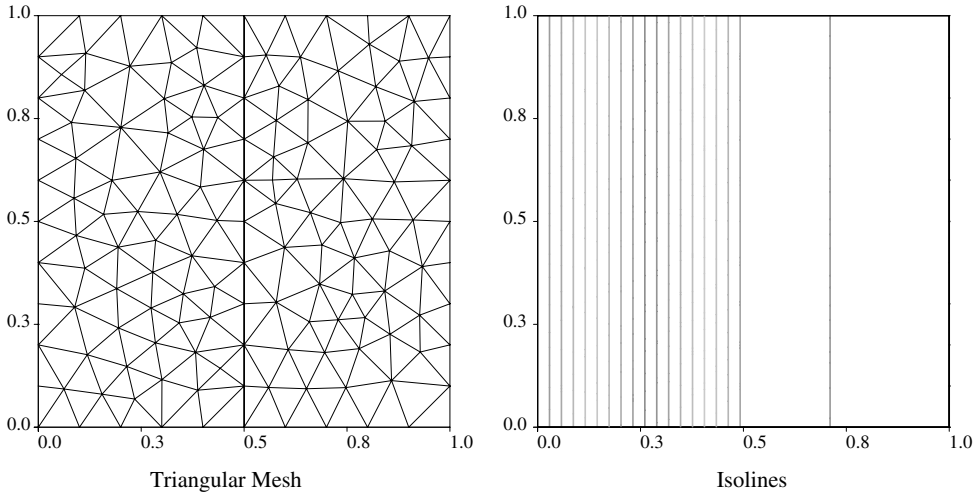

Fig. 12. A discontinuous conductivity problem.

The conductivity $D = D(x, y)$ is discontinuous and given by

$$\begin{aligned} &0 \leqslant x \leqslant \frac{1}{2} \quad D = D_1, \\ &\frac{1}{2} \leqslant x \leqslant 1 \quad D = D_2. \end{aligned} \tag{83}$$

We set $S = 0$ and the exact solution is

$$\begin{aligned} &0 \leqslant x \leqslant \frac{1}{2} \quad u(x,y) = a + bx + cy, \\ &\frac{1}{2} \leqslant x \leqslant 1 \quad u(x,y) = a - b\frac{D_2 - D_1}{2D_2} + b\frac{D_1}{D_2}x + cy. \end{aligned} \tag{84}$$

A straightforward computation shows that the normal flux to the interface is continuous and equal to $D_1 b$. The tangential components is $D_1 c$ on the left side and $D_2 c$ on the right side of the interface.

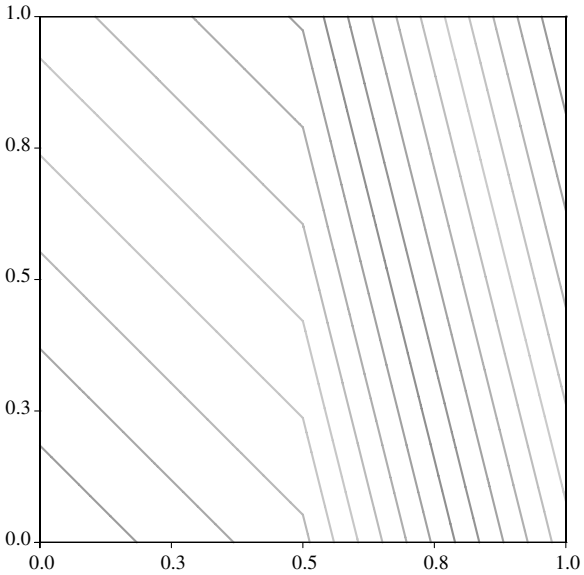

Fig. 13. Isolines for the discontinuous tangential flux problem.

The numerical results are obtained using $D_1 = 4$, $D_2 = 1$, $a = b = c = 1$ and the same triangular mesh as in the previous case. We apply Dirichlet boundary conditions which are directly deduced from the analytical solution (84).

As previously, the asymptotic errors obtained are equal to zero up to machine precision. Our scheme reproduces exactly the linear solution. The calculated isolines of the numerical steady-state solution are shown in Fig. 13.

5.1.3. A non linear problem

The aim of this test case is to perform a convergence analysis. The problem is characterized by a constant conductivity $D = 1$ and the source term $S(x,y) = x^2$. The boundary conditions are given by (80). The non linear analytical solution is given as

$$u(x,y) = \left(1 + \frac{1}{12D}\right)x - \frac{1}{12D}x^4. \tag{85}$$

We compute three numerical solutions on three triangular unstructured meshes which are composed of 254, 988 and 3984 cells. These meshes are displayed in Fig. 14. The convergence analysis is presented in Table 1. In addition the two asymptotic errors versus the mesh resolution are displayed in Fig. 15. We have also plotted the theoretical second order convergence error. It is clear that the convergence rate is second order in both the max and the l_2 norms.

5.2. Quadrangular mesh

5.2.1. Linear problem on parallelogram cells

The aim of this test is to show that our scheme preserves linear solution on quadrangular grids which are composed of parallelogram cells. We solve the diffusion Eq. (79) on a domain which is obtained from the unit square $0 \leqslant \xi,\eta \leqslant 1$ using the map

$$\begin{aligned} x(\xi,\eta) &= \xi + \eta, \\ y(\xi,\eta) &= \eta. \end{aligned} \tag{86}$$

This map transforms the unit square into a parallelogram. The conductivity is constant over the domain $D(x,y) = 1$. The boundary conditions are given by

$$\begin{aligned} &D\frac{\partial u}{\partial y} = -D \quad \text{at } y = 0, \quad D\frac{\partial u}{\partial y} = -D \quad \text{at } y = 1, \\ &u = 0 \quad \text{at } x - y = 0, \quad u = 1 \quad \text{at } x - y = 1. \end{aligned} \tag{87}$$

The analytical solution is

$$u(x,y) = x - y. \tag{88}$$

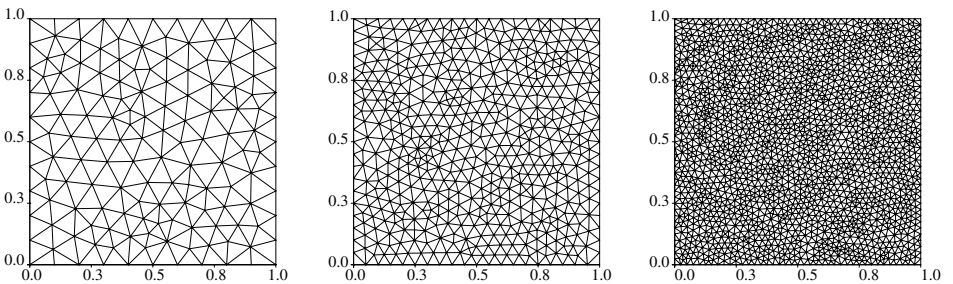

Fig. 14. Triangular grids for convergence analysis.

Table 1
Convergence analysis for the non linear problem on triangular mesh

h	$E^h_{\max}$	$q_{\max}$	$E^h_{l_2}$	q_{l_2}
$6.27D-2$	$8.09D-4$	1.61	$3.34D-4$	2.05
$3.18D-2$	$2.71D-4$	2.18	$8.29D-5$	2.06
$1.58D-2$	$5.91D-5$	–	$2.06D-5$	

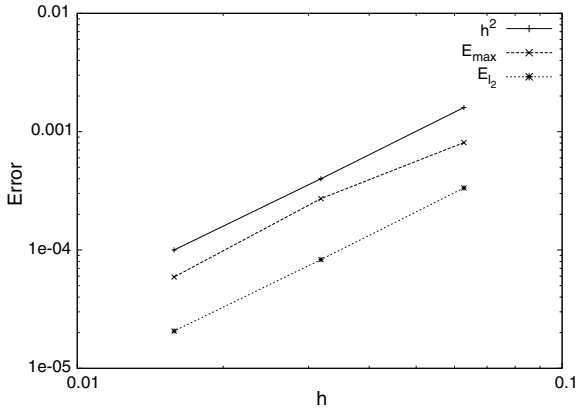

Fig. 15. Asymptotic errors in logarithmic scale for the non linear problem.

The mesh used for the computations is displayed in Fig. 16. It is composed of 100 parallelogram cells. The isolines which are shown in Fig. 16 are parallel straight lines. Thus, the scheme preserves the linear solution up to machine precision. We will see in the next paragraph that this property is no longer verified for non parallelogram cells.

5.2.2. Linear problem on a quadrangular distorted mesh

We solve the standard diffusion problem defined on the unit square. We use a constant conductivity $D(x,y) = 1$ and the boundary conditions are those given by (80). The analytical solution is

$$u(x,y) = x. \tag{89}$$

The aim of this problem is to test the accuracy of our scheme for a sequence of distorted grids of three different types. As in [25], we introduce the smooth grids given by the transformation

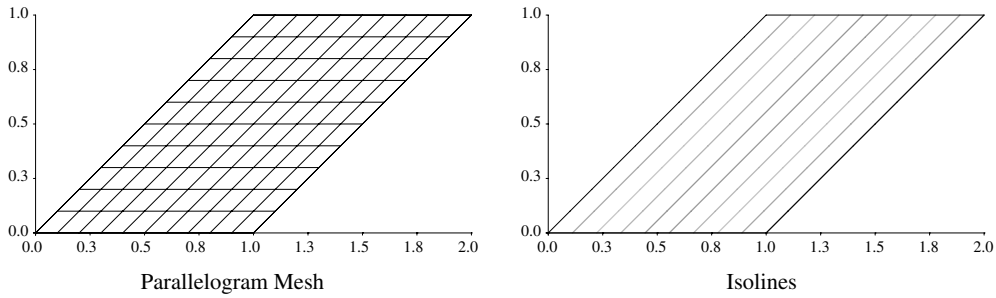

Fig. 16. Linear problem on parallelogram cells.

$$x(\xi,\eta) = \xi + a_0 \sin(2\pi\xi)\sin(2\pi\eta),$$
$$y(\xi,\eta) = \eta + a_0 \sin(2\pi\xi)\sin(2\pi\eta). \tag{90}$$

We have displayed the three smooth grids obtained by this map for $a_0 = 0.1$ in Fig. 17(top). We also introduce the highly irregular Kershaw grid, see [10]. The three Kershaw grids are shown in Fig. 17(middle). Finally, in

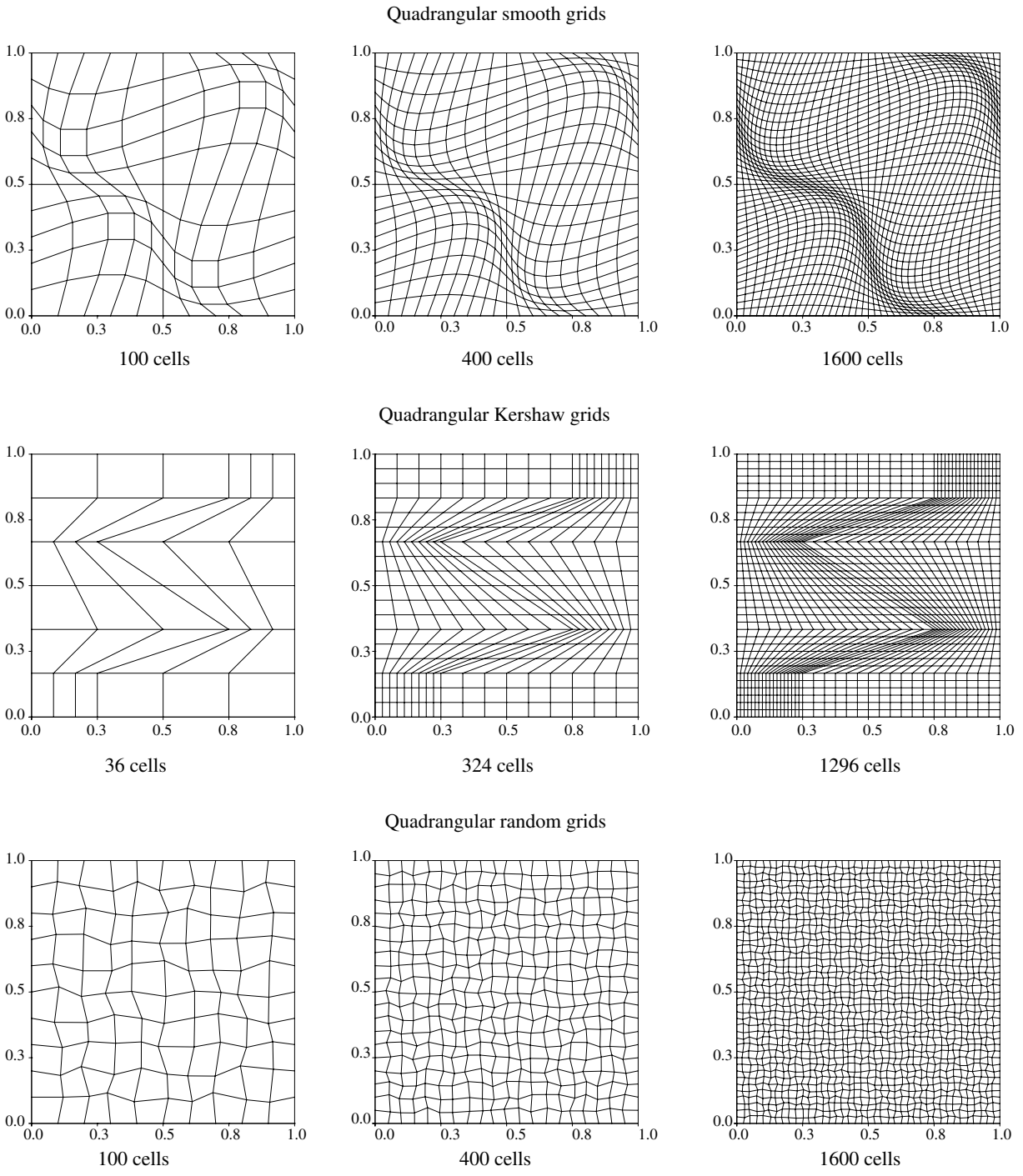

Fig. 17. Girds for convergence analysis.

order to demonstrate the accuracy of our scheme as a function of the mesh size on "random" meshes, we introduce the random grids displayed in Fig. 17(bottom). These meshes are obtained from a uniform orthogonal mesh by randomly displacing each interior nodes. Specifically, given an initial uniform cell width of size h, each node is placed at a random position on a circle of radius $0.2h$, centered at the initial position of the node.

The convergence analysis for the smooth grids is presented in Table 2(top). It appears that the convergence rate is almost second order in both the max and the l_2 norms. We point out that $q_{\max}$ and q_{l_2} are obtained using (78). We show the convergence analysis results for the Kershaw grids in Table 2(middle). It appears that the convergence rate is also very close to second order. Finally, we show the convergence analysis results for the random grids in Table 2(bottom). These results show a very low order of convergence on random grids

5.2.3. Non linear problem on a quadrangular distorted mesh

In order to corroborate the previous results, we make a convergence analysis on the non linear problem which has been presented in Section 5.1.3. As previously, we test the accuracy of our scheme on a sequence of distorted grids of three types: smooth, Kershaw and random. The convergence analysis results for the smooth grids are displayed in Table 3(top). For the Kershaw grids, we present the convergence analysis data in Table 3(middle). Finally, the convergence analysis for random grids is presented in Table 3(bottom). It appears that the non linear results confirm the linear one. Our scheme shows a quasi second order behavior on distorted grids such as smooth and Kershaw grids. However, we obtain a convergence rate lower than one for random grids.

5.2.4. Discontinuous tangential flux

We make a convergence analysis on the discontinuous tangential flux problem which has been defined in Section 5.1.2. For this problem, we use smooth and random grids which have been generated as usual. We notice that the nodes located on the interface keep their initial positions. The convergence analysis data for the smooth grids are displayed in Table 4(left). They show a quasi second order convergence rate. We perform a similar study for the random grids and we obtain as previously a convergence rate lower than one.

5.2.5. Comparison with the Kershaw scheme on a non linear test case

In this paragraph we propose an analytical test case for which we make comparison between our new scheme and the Kershaw scheme. This test case corresponds to the stationary solution of (79) with $D = 1$ and homogeneous Neumann boundary conditions. The source term is defined by

$$S(x, y) = x + u(x, y).$$

Table 2
Convergence analysis for the linear problem on quadrangular distorted mesh

h	$E^h_{\max}$	$q_{\max}$	$E^h_{l_2}$	q_{l_2}
Smooth grids				
$1.0D-1$	$6.13D-3$	1.72	$2.31D-3$	1.83
$5.0D-2$	$1.86D-3$	1.89	6.48D−4	1.96
$2.5D-2$	$5.06D-4$	–	$1.67D-4$	–
Kershaw grids				
$1.67D-1$	$4.07D-2$	1.52	$1.81D-2$	1.85
$5.55D-2$	$7.61D-3$	1.66	$2.35D-3$	1.92
$2.78D-2$	$2.41D-3$	–	$6.21D-4$	–
Random grids				
$1.0D-1$	$1.96D-3$	0.38	$6.05D-4$	0.76
$5.0D-2$	$1.51D-3$	0.66	$3.57D-4$	0.55
$2.5D-2$	$9.55D-4$	–	$2.43D-4$	–

Table 3
Convergence analysis for the non linear problem on quadrangular distorted mesh

h	$E^h_{\max}$	$q_{\max}$	$E^h_{l_2}$	q_{l_2}
Smooth grids				
$1.0D-1$	$6.17D-3$	1.31	$2.49D-3$	1.84
$5.0D-2$	$1.90D-3$	1.87	$6.93D-4$	1.96
$2.5D-2$	$5.19D-4$	–	$1.78D-4$	–
Kershaw grids				
$1.67D-1$	$4.29D-2$	1.5	$1.86D-2$	1.84
$5.55D-2$	$8.17D-3$	1.66	$2.44D-3$	1.93
$2.78D-2$	$2.60D-3$	–	$6.43D-4$	–
Random grids				
$1.0D-1$	$1.92D-3$	0.37	$6.21D-4$	0.69
$5.0D-2$	$1.48D-3$	0.18	$3.84D-4$	0.15
$2.5D-2$	$1.31D-3$	–	$3.46D-4$	–

Table 4
Convergence analysis for the discontinuous tangential flux problem on quadrangular mesh

h	$E^h_{\max}$	$q_{\max}$	$E^h_{l_2}$	q_{l_2}
Smooth grids				
$1.0D-1$	$1.32D-2$	1.83	$4.06D-3$	1.83
$5.0D-2$	$3.72D-3$	1.94	$1.14D-3$	1.95
$2.5D-2$	$9.69D-4$	–	$2.96D-4$	–
Random grids				
$1.0D-1$	$6.71D-3$	0.67	$2.03D-3$	0.87
$5.0D-2$	$4.21D-3$	0.5	$1.11D-3$	0.77
$2.5D-2$	$2.97D-3$	–	$6.49D-4$	–

With these data the stationary solution is

$$u(x,y) = -x + \left(\frac{\cos(1)-1}{\sin(1)}\right)\cos(x) + \sin(x).$$

This test case is characterized by homogeneous Neumann boundary conditions. This test case has been designed in order to use only homogeneous boundary conditions. Like this, we avoid the difficulties inherent to the discretization of Dirichlet boundary conditions with the Kershaw scheme. The convergence analysis results for the smooth grids (Table 5) and the Kershaw grids (Table 6) clearly demonstrate a second order of convergence for our scheme and a first order convergence for the Kershaw scheme.

On the other hand, results for random grids (Table 7) suggest that our method and the Kershaw scheme do not converge on such meshes. This last comment is in agreement with results obtained for the Kershaw scheme in [17]. We point out that the behavior of our method on random grids is very similar to that of the symmetric

Table 5
Comparison between our scheme and the Kershaw scheme for the non linear problem on smooth quadrangular grids

h	$E^h_{\max}$	$q_{\max}$	$E^h_{l_2}$	q_{l_2}
Our scheme				
$1.0D-1$	$1.56D-3$	1.67	$6.47D-4$	1.73
$5.0D-2$	$4.90D-4$	1.89	$1.95D-4$	1.92
$2.5D-2$	$1.32D-4$	–	$5.14D-5$	–
Kershaw scheme				
$1.0D-1$	$3.82D-3$	0.77	$1.27D-3$	0.91
$5.0D-2$	$2.24D-3$	0.94	$6.75D-4$	1.04
$2.5D-2$	$1.17D-3$	–	$3.28D-4$	–

Table 6
Comparison between our scheme and the Kershaw scheme for the non linear problem on Kershaw quadrangular grids

h	$E^h_{\max}$	$q_{\max}$	$E^h_{l_2}$	q_{l_2}
Our scheme				
$1.67D{-}1$	$9.43D{-}3$	1.63	$5.49D{-}3$	1.88
$5.55D{-}2$	$1.56D{-}3$	1.81	$6.89D{-}4$	1.97
$2.78D{-}2$	$4.45D{-}4$	–	$1.77D{-}4$	–
Kershaw scheme				
$1.67D{-}1$	$2.33D{-}2$	0.47	$1.61D{-}2$	0.5
$5.55D{-}2$	$1.38D{-}2$	0.69	$9.38D{-}3$	0.76
$2.78D{-}2$	$8.57D{-}3$	–	$5.55D{-}3$	–

Table 7
Comparison between our scheme and the Kershaw scheme for the non linear problem on random quadrangular grids

h	$E^h_{\max}$	$E^h_{l_2}$
Our scheme		
$1.0D{-}1$	$5.0D{-}4$	$1.91D{-}4$
$5.0D{-}2$	$4.53D{-}4$	$2.36D{-}4$
$2.5D{-}2$	$5.35D{-}4$	$3.52D{-}4$
Kershaw scheme		
$1.0D{-}1$	$9.96D{-}4$	$4.04D{-}4$
$5.0D{-}2$	$1.02D{-}3$	$5.78D{-}4$
$2.5D{-}2$	$9.85D{-}4$	$6.42D{-}4$

MPFA method described in [5]. Namely, on random grids symmetric MPFA method suffers reduction or loss of convergence. Our scheme is currently used in the context of Arbitrary Lagrangian Eulerian computations. In this context, the rezoning phase always produces smooth distorted grids for which our scheme shows a quasi second order convergence. Consequently, the loss of convergence on random grids has no impact on such computations.

5.3. A non linear thermal wave

We consider a non linear thermal wave which is the solution of the following diffusion equation:

$$\rho C \frac{\mathrm{d}u}{\mathrm{d}t} - \nabla \cdot (D(u)\nabla u) = 0,$$

where we set $\rho = 1$ and $C = 1$. The non linear diffusion coefficient is given by

$$D(u) = u^{\frac{5}{2}}.$$

This type of non linearity is encountered in plasma physics for electron energy transport, see [28]. The diffusion equation is solved on a cylindrical domain Ω characterized by $r \in [0,1]$ and $\theta \in [0, \frac{\pi}{2}]$ knowing that $r = \sqrt{x^2 + y^2}$ and $\theta = \arctan\frac{y}{x}$ where (x, y) denotes the Cartesian coordinates of a generic point inside the domain. The initial condition u^0 is given by

$$u^0(x, y) = 1.$$

There are symmetric boundary conditions along $x = 0$ and $y = 0$ and we impose the normal flux $\Phi^\star = 1000$ on the circular boundary defined by $r = 1$. We compute the solution until time $T = 3.25 \times 10^{-3}$. At this time a heat wave has propagated into the cold medium. This wave is characterized by a sharp transition zone displaying a strong temperature gradient. Due to the boundary conditions and the geometry of the domain, the solution of the diffusion equation exhibits a cylindrical symmetry, namely $u \equiv u(r)$.

First, we compute the reference numerical solution using a 50×20 polar grid which is displayed in Fig. 18. We apply a strong distortion to this regular polar grid using the following transformation:

$$x' = \sqrt{r}\cos\theta,$$
$$y' = r\sin\theta.$$

The resulting distorted grid is shown in Fig. 18. Then, with this distorted grid, we compute the numerical solution using the classical five-point scheme, the Kershaw scheme [10] and our new scheme. We have plotted the five-point scheme solution at time $T = 3.25 \times 10^{-3}$ in Fig. 19. We notice that we have displayed the temperature of each cell as function of the radius computed at the centroïd of the cell. The five-point scheme exhibits a well known default, namely the temperature front is aligned with the mesh distortion. Therefore, the numerical solution has lost its cylindrical symmetry feature. This is corrected by using the Kershaw scheme or our new scheme, as it can be seen in Fig. 20. Those two schemes are nine-point schemes and give the expected one-dimensional solution. In order to compare more precisely these two schemes, we have displayed in Fig. 21 an enlarged view of the thermal front. We notice that the Kershaw scheme produce some temperature undershoots located in the cold medium in front of the thermal wave contrarily to our scheme.

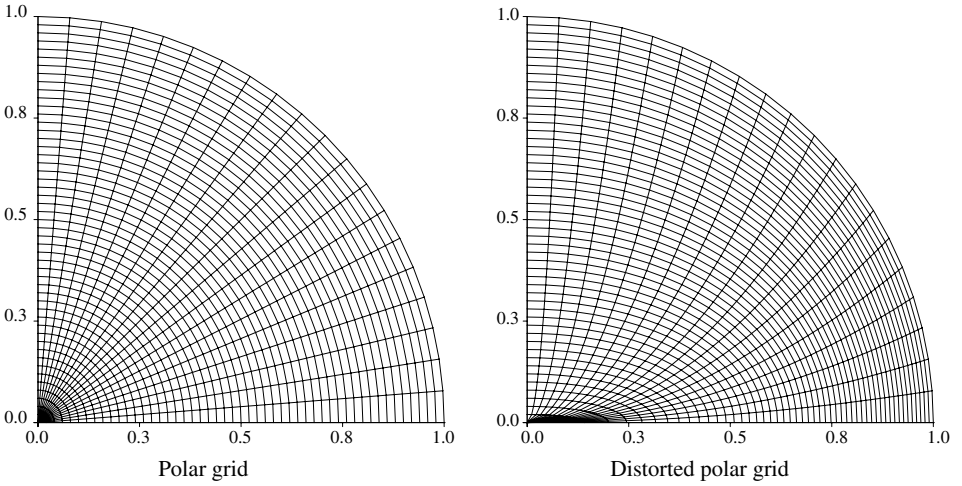

Fig. 18. Polar grids.

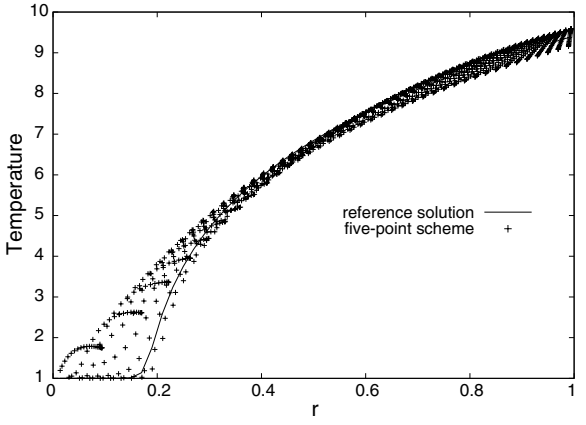

Fig. 19. Five-point scheme: temperature profiles at $T = 3.25 \times 10^{-4}$.

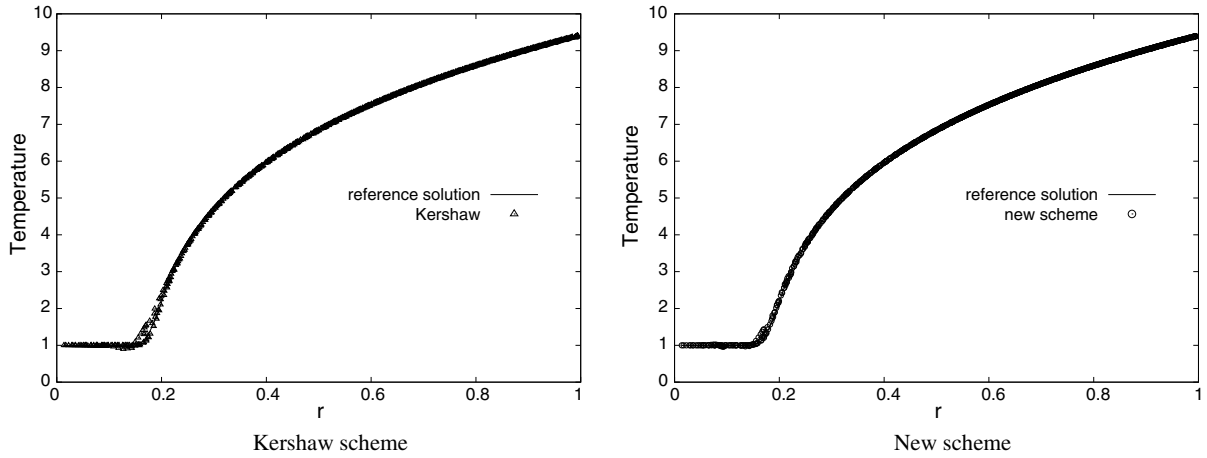

Fig. 20. Temperature profiles at $T = 3.25 \times 10^{-4}$.

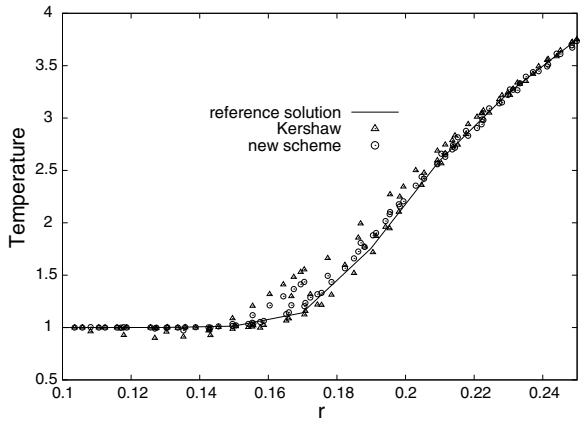

Fig. 21. Kershaw and new scheme: zoom at the thermal front.

6. Conclusions

We have developed a new cell-centered diffusion scheme on two-dimensional unstructured meshes. This scheme has only cell-center unknowns, a local stencil and yields a sparse banded diffusion matrix which is symmetric positive definite. Moreover, for triangular grids, our algorithm preserves linear solutions and gives second order accuracy. For quadrangular grids, we have shown that the accuracy of this scheme is almost second order except for non smooth grids.

In the future, we intend to investigate improvements of the quadrangular formulation in order to obtain exact second order accuracy. We shall examine also non-isotropic materials.

Acknowledgement

The authors thank Guy Schurtz for fruitful discussions about the Kershaw scheme and for providing us with the ICCG solver.

References

[1] I. Aavatsmark, An introduction to multipoint flux approximations for quadrilateral grids, Comput. Geosci. 6 (2002) 405–432.
[2] I. Aavatsmark, T. Barkve, O. Boe, T. Mannseth, Discretization on unstructured grids for inhomogeneous, anistropic media. Part I: derivation of the methods, SIAM J. Sci. Comput. 19 (1998) 1700–1716.
[3] I. Aavatsmark, T. Barkve, O. Boe, T. Mannseth, Discretization on unstructured grids for inhomogeneous, anistropic media. Part II: discussion and numerical results, SIAM J. Sci. Comput. 19 (1998) 1717–1736.
[4] I. Aavatsmark, G.T. Eigestad, R.A. Klausen, Numerical convergence of the MPFA O-method for general quadrilateral grids in two and three dimensions, in: D.N. Arnold, P.B. Bochev, R.B. Lehoucq, R.A. Nicolaides, M. Shashkov (Eds.), Compatible Spatial Discretizations, IMA Vol. Ser., Springer, 2006.
[5] I. Aavvatsmark, G.T. Eigestad, R.A. Klausen, M.F. Wheeler, I. Yotov, Convergence of a symmetric MPFA method on quadrilateral grids. Technical Report TR-MATH 05-14, University of Pittsburgh, 2005.
[6] P.I. Crumpton, G.J. Shaw, A.F. Ware, Discretisation and multigrid solution of elliptic equations with mixed derivatives terms and strongly discontinuous coefficients, J. Comp. Phys. 116 (1995) 343–358.
[7] M.G. Edwards, C.F. Rogers, Finite volume discretization with imposed flux continuity for the general tensor pressure equation, Comput. Geosci. 2 (1998) 259–290.
[8] R. Eymard, T. Gallouët, R. Herbin, Finite Volume methodsHandbook of Numerical Analysis, Elsevier Sciences, 2000.
[9] J. Hyman, J.E. Morel, M. Shashkov, S. Steinberg, Mimetic finite difference methods for diffusion equations, Comput. Geosci. 6 (2002) 333–352.
[10] D.S. Kershaw, Differencing of the diffusion equation in lagrangian hydrodynamic codes, J. Comp. Phys. 39 (1981) 375–395.
[11] R.A. Klausen, T.F. Russell, Relationships among some locally conservative discretization methods wich handle discontinuous coefficients, Comput. Geosci. 8 (2004) 341–377.
[12] Y. Kuznetsov, K. Lipnikov, M. Shashkov, The mimetic finite difference method on polygonal meshes for diffusion-type problems, Comput. Geosci. 8 (2004) 301–324.
[13] P. Lascaux, R. ThéodorAnalyse Numérique matricielle appliquée à l'art de l'ingénieur, vol. II, Dunod, 2000.
[14] K. Lipnikov, J.E. Morel, M. Shashkov, Mimetic finite difference methods for diffusion equations on non-othogonal non-conformal meshes, J. Comp. Phys. 199 (2004) 589–597.
[15] K. Lipnikov, M. Shashkov, I. Yotov, Local flux mimetic finite difference methods, Technical Report LA-UR-05-8364, Los Alamos National Laboratory, 2005.
[16] R. Liska, M. Shashkov, V. Ganzha, Analysis and optimization of inner products for mimetic finite difference methods on triangular grid, Math. Comput. Simulat. 67 (2004) 55–66.
[17] J.E. Morel, J.E. Dendy, M.L. Hall, S.W. White, A cell-centered lagrangian-mesh diffusion differencing scheme, J. Comp. Phys. 103 (1992) 286–299.
[18] J.E. Morel, R.M. Roberts, M. Shashkov, A local support-operators diffusion discretization scheme for quadrilateral r-z meshes, J. Comp. Phys. 144 (1998) 17–51.
[19] G.A. Moses, J. Yuan, Radiation diffusion in draco using kershaw difference scheme, Technical Report UWFDM-1213, Fusion Technology Institute. University of Wisconsin, 2003.
[20] J.D. Moulton, T.M. Austin, M. Shashkov, J.E. Morel, Mimetic preconditionners for mixed discretizations of the diffusion equation. Available from: <http://www.ima.umn.edu/complex/spring/discretization.html> LA-UR-01-807.
[21] C. Le Potier, A finite volume method for the approximation of highly anisotropic diffusion operators on unstructured meshes, in: Finite Volumes for Complex Applications IV, Marrakech, Marocco, 2005.
[22] C. Le Potier, Schéma volume finis pour des opérateurs de diffusion fortement anisotropes sur des maillages non structurés, C.R. Acad. Sci. Paris Ser. I 340 (2005) 921–926.
[23] M. Shashkov, Conservative Finite-Difference Methods on General Grids, CRC Press, 1996.
[24] M. Shashkov, S. Steinberg, Support-operator finite-difference algorithms for general elliptic problems, J. Comp. Phys. 118 (1995) 131–151.
[25] M. Shashkov, S. Steinberg, Solving diffusion equations with rough coefficients in rough grids, J. Comp. Phys. 129 (1996) 383–405.
[26] V. Subramanian, J.B. Perot, High-order mimetic methods for unstructured meshes, J. Comp. Phys. (2006).
[27] J.-M. Thomas, D. Trujillo, Mixed finite volume methods, Int. J. Numer. Meth. Eng. 46 (1999) 1351–1366.
[28] Y.B. Zel'dovich, Y.P. RaizerPhysics of Shock Waves and High-Temperature Hydrodynamic Phenomena, vol. 1, Academic Press, 1966.